UNIVERSITY OF OKLAHOMA

GRADUATE COLLEGE

POROUS SHAPE MEMORY POLYMER NANOCOMPOSITES: SYNTHESIS, CHARACTERIZATION, AND POTENTIAL BIO-APPLICATION

A THESIS

SUBMITTED TO THE GRADUATE FACULTY

In partial fulfillment of the requirements for the

Degree of

MASTER OF SCIENCE

By

JISHAN LUO

Norman, Oklahoma

2019

POROUS SHAPE MEMORY POLYMER NANOCOMPOSITES: SYNTHESIS, CHARACTERIZATION, AND POTENTIAL BIO-APPLICATION

A THESIS APPROVED FOR THE

SCHOOL OF AEROSPACE AND MECHANICAL ENGINEERING

BY THE COMMITTEE CONSISTING OF

Dr. Yingtao Liu, Chair

Dr. Mrinal Saha

Dr. Chung-Hao Lee

Table of Content

Nomenclature

CNT	Carbon nanotube (Multi-walled carbon nanotube)
DMA	Dynamic mechanical analysis
DSC	Differential scanning calorimetry
GDC	Guglielmi detachable coil
HDI	Hexamethylene diisocyanate
HPED	N,N,N’,N’-tetrakis(2-hydroxypropyl) ethylenediamine
ICA	Intracranial aneurysm
SEM	Scanning electron microscopy
SMP	Shape memory polymer
CNT/SMP	Carbon nanotube/Shape memory polymer composites
TEA	Triethanolamine
T_g	Glass transition temperature
TGA	Thermal gravimetric analysis

List of Figures

Acknowledgement

Firstly, I would like to express my deepest gratitude to Dr. Yingtao Liu in the School of Aerospace and Mechanical Engineering at the University of Oklahoma, for providing me the great opportunity to become a member in his research group, and all the guidance and support he offered to me during my graduate life. I really appreciate that Dr. Liu's guidance, patience, encouragement, insightful commentary, and creative ideas helped me to pursue my dream at OU. This work would not be done without his support and guidance.

I also want to thank Dr. Mrinal Saha, his support, and encouragement inspired my enthusiasm to work hard for my research. I would also like to thank Dr. Chung-Hao Lee, for his support, and insightful ideas for my research. Thank Dr. Zahed Siddique for offering me the great opportunity to communicate with excellent researchers in IMECE conference. Thank Dr. M. Cengiz Altan for letting me use his lab equipment. Thank Dr. Preston Larson for training me to operate sputter coating for scanning electron microscopy.

I am also grateful for my lab mates, Jingyu wang, Blake Herren, Colin Bray, Ryan Cowdrey, for their help and support for my project. I would like to thank Dr. Mehrad Amirkhosravi, Mohammad Charara, Wenyuan Luo, for their advice and help for my research.

I also appreciate for all staff of Aerospace and Mechanical Engineering department, Bethany Burklund, Melissa Foster, Ellen McKenzie, Martina Ferguson, Rebeka Morales, Billy Mays, and Greg Williams, for their support and assistance during my graduate life here.

Lastly, thank all my family members for their love, sacrifices, and support. I would not be here without their encouragement and financial support. I want to thank my boyfriend, for his love

and selfless support, motivating me to work hard. It is their endless love and support that help me get through my graduate life, and step into a bright future.

Abstract

Porous shape memory polymers (SMPs) are the smart materials which attract significant interests in the fields such as aerospace, civil engineering, electrical engineering, and biomedical device. Porous SMPs have low recover stress, excellent recover strain, low density, and biocompatibility, making it a great potential candidate in the treatment of Intracranial Aneurysms (ICAs). In this thesis, pristine SMP foams, CNT/SMP nanocomposite foams, and 3D printed CNT/SMP nanocomposite scaffolds are synthesized and characterized. The pristine SMP foams have a porosity of 85.7% and a shear fracture around 90% of the strain, which have significantly higher elastic deformation at the temperature above glass transition temperature. Compared with the pristine SMP foams, CNT/SMP nanocomposite foams have good conductivity, which enables it to use joule-heating method to trigger the compressed foams to recover to the original shape in much less time. Using 3D printing technique to fabricate the CNT/SMP nanocomposite scaffolds has greatly reduced the manufacturing time from 120 hours to 30 minutes and can personalize the geometry of printed complex structures. Designing tunable configuration of electroactive CNT/SMP nanocomposites enables this study advantageous for the potential medical device design for treating the ICAs.

Chapter 1 Introduction

1.1 Porous shape memory polymers

Shape memory polymers (SMPs) are the smart materials that have the ability to recover from a temporarily deformed shape to the original shape by responding to the external stimuli, such as heat, light and electrical field [1-3]. Recently, SMPs have attracted significant interests in many engineering fields, such as biomedical device, aerospace, civil engineering, electrical engineering and textile industry due to the excellent properties including lightweight, high capacity of elastic deformation, tunable glass transition temperature and lower cost [4-9]. Compared to the solid SMPs, the shape memory behavior of porous SMPs are strengthened due to the increased compressibility and reduced density, which are desired material to have broad applications in aerospace industry and biomedical field [10,11].

The form of porous SMPs can be varied by responding to the heat temperature switching between above and below the glass transition temperature (T_g). The state of SMPs is rubbery and soft when the temperature of external heat stimulus is high than T_g, and the state is rigid and stiff when the temperature is lower than T_g. The mechanical properties of SMPs including strength and modulus change greatly for the SMPs in two states.

The typical thermo-mechanical behavior of SMPs is demonstrated in Figure 1-1. After curing, the shape of SMPs is permanently memorized which is called original shape. When the temperature of external stimulus is higher than T_g, the shape can be freely packed.

Then the temporarily deformed SMPs is cooled by decreasing the temperature below the T_g, so the shape is temporarily memorized. If the SMPs need to recover to the original shape, shape will start changing by increasing the temperature over T_g. By cooling down the SMPs, the SMPs will be clocked back to original shape and mechanical properties again.

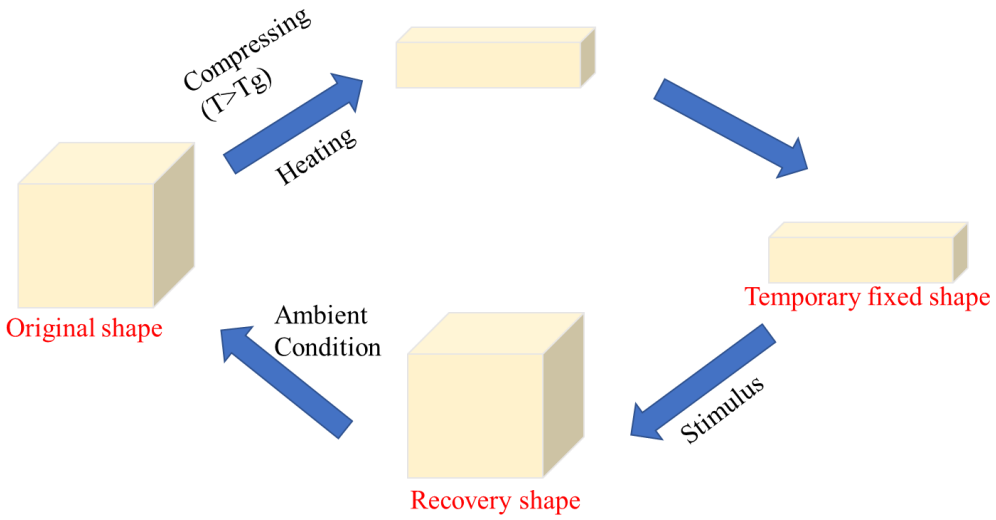

Figure 1-1 Shape recovery effect of SMPs.

1.2 Fabrication of porous SMPs

Porous SMPs have been fabricated by various techniques including gas foaming, sacrificial template and 3D printing[12-14]. These techniques can significantly influence the size and uniformity of pores which determine the structure and behavior of SMPs.

1.2.1 Gas foaming

Chemical and physical blowing agents can be used to generate bubbles inside the SMPs for developing the pores [15-19]. Gas will be generated when the chemical blowing

agent react with the SMPs, and bubbles will be formed due to the phase transition of SMPs caused by the physical blowing agent.

Water can be used as the chemical blowing agent that react with isocyanate monomers for synthesizing the porous SMPs. Carbon dioxide gas will be generated during the foam blowing which will create pore structure and interconnectivity inside the SMPs. The type and concentration of foaming agent determine the size and quality of pores. Pooja et al. [20] varied the molar ratio of water, HDI, HPED and TEA to create polyurethane based SMP foams of highly crosslinked and ultra-low density. The T_g can be customized between 45 °C and 70 °C and the expansion of high volume can be as many as 70 times.

For the physical blowing, changes of pressure and temperature can cause a separation of gas phase from the solution in supersaturation. When the temperature and pressure are above the critical point, supercritical fluids can be filled with carbon dioxide which is an inert gas. Physical blowing agent like the supercritical carbon dioxide is saturated inside the polymer when it is at high temperature but below the polymer melting temperature and high pressure. The polymer is in rubbery and soft state as the T_g decreases. Then decreasing the pressure of system will make a new equilibrium of thermodynamic. Cell growth and instantaneous nucleation will occur due to the oversaturated carbon dioxide inside the rubbery polymer. Porous structure will be achieved due to the evaporation of carbon dioxide out of the system, and the polymer is glassy.

1.2.2 Sacrificial template

Solid particles including sugar and salt are formed as sacrificial template which can be leached out of polymer matrix[16,21-26]. The skeleton structure with interconnected bonding inside can be obtained by sacrificial template which works as porogenic agent. Polymer solution is poured onto the template and penetrates the skeleton slowly. Template is removed by immersing the template/polymer composites in solvent such as water, leading to the dissolving of solid particles and leaving the porous polymer structures. The porosity, geometry and morphologies of pores can be tailored by varying the diameter and shape of solid particles.

Wang et al.[22] used the sugar to prepare the sacrificial template by compressing certain amount of sugar in a silicon rubber mold with a slight amount water which could enhance the interfacial bonding inside the template. Prepared polymer solution infiltrated through the template and template was removed by later water dissolving. The average pore size and density of SMP foam were 480um and 0.168g/cm^3.

Chai et al. [27] prepared the sacrificial templates by two size of salt particles including 150-300 um and 300-500 um. The salt templates were poured by the polymer solution which were curing in later oven processing. Water was replaced every 6h to remove the salt particles when the template/polymer composites were immersed in water solvent. They found that the pore size of foams could be controlled by the size of salt particles, meaning that small salt particles resulted in foam of small pore, and large salt particles leaded to the large pores and thick cell walls.

1.2.3 3D printing

There are drawbacks for the previous fabrication techniques of porous SMPs that the design of porous SMP structures is difficult to be customized and whole process takes very long time as the majority of time is spent on the dissolving of solid particles. Also the facilities and equipment to achieve the environment of high temperature and pressure is high cost and dangerous.

The emergence of 3D printing becomes a perfect technique due to its flexibility in designing complex structures, customization of shape and additive manufacturing approach eliminating use of raw materials[28-39]. Common 3D printing techniques including inkjet and digital light processing are used to print porous SMP structures because they are low cost and relatively fast [40,41].

Mu et al. [31] prepared the ink by mixing the sacrificial salt particulates and photocurable resin together, then printed the objects by a customized DLP printer. Porous polymeric structures were obtained after the salt particulates were removed. They also used this method to print the polymeric cube with shape memory effect. They found that the size of salt particulates determined the pore size and this method was simple to create complicated porous structures.

1.3 Application of porous SMPs

Due to the unique properties including high compression capacity and shape memory behaviors, porous SMPs have broad applications in two main fields such as aerospace and biomedical device[11,19,42].

1.3.1 Aerospace

Expandable and deployable structures which have low density and high compressive capability are demanded in aerospace for the fuel efficiency and specific performance. Porous SMPs play an important role in this field due to its reliability, simplicity, low cost, extremely high full/stowed volume ratio and great resistance to impact and radiation [5,11,43-45]. The solar heating will benefit the deployment of porous SMP structures of thermally activation in space. The self-healing properties of SMPs can make SMP composite structure suffer more the potential impact damage and automatically repair the structures by responding to the external stimulus. Ability of energy absorption of porous SMPs makes it protect the structures from serious object striking

Fabrizio et al.[46] produced the actuator based on the SMP foams for the potential application in International Space Station. The density and foaming ratio of SMP foams were 0.36 g/cm^3 and 4, respectively. The actuation loads relating to the temperature were measured by multiple recovery tests. After the optimization of fabrications, certain type of actuator was tested in International Space Station with encouraging results.

1.3.2 Biomedical device

Numerous biomedical applications of porous SMPs have been reported mainly in two fields including vessel embolization and tissue reconstruction [6,19,47-51]. Excellent shape recovery, high surface to volume ratio and tortuous flow of porous SMP devices lead to the application of embolic vascular devices. The scaffolds offered by SMP matrix can be helpful for the tissue growth and give the locations for the cells to regenerate the tissues

Singhal et al. [19] synthesized the biodegradable foams of SMP for embolic application in biomedical engineering. By tuning the ratio of reaction monomers, the ultra-low densities of SMP foams were obtained ranging from 0.02 to 0.093 g/cm^3.The cell morphology of SMP foams were uniform which had excellent shape recovery.

Mao et al. [6] produced the biodegradable nanofibrous structures by combining the SMPs and biomimicking nanofibers using electrospinning. They varied the ratio of monomers to achieve the fibers with different T_g and fineness. The novel structure could be used for surgical implantation with minimal invasion and improving the efficiency of repairing and regenerating tissues.

1.4 Treatments of intracranial aneurysms

Intracranial Aneurysms (ICAs) are the localized dilations of arteries in brain vasculature with a prevalence of roughly 5% in population [52]. The incidental rupture of aneurysm will lead to the subarachnoid hemorrhage that causes the death of people. Currently, there are several treatments for ICAs including surgical clipping and endovascular coiling [53-57]. Porous SMP structures are investigated as the potential treatment for this disease [21,58-64].

1.4.1 Surgical clipping

Surgical clipping was first performed by Walter Dandy in 1937 [65]. A silver clip that blocked the blood flow to the bulge part was affixed across the aneurysm neck as shown in Figure 1-2. Before the surgical clipping, a craniotomy has to be done so that the

aneurysm can be exposed. As the craniotomy has high risk, this method may not be friendly to the old people and the operation cost is expensive.

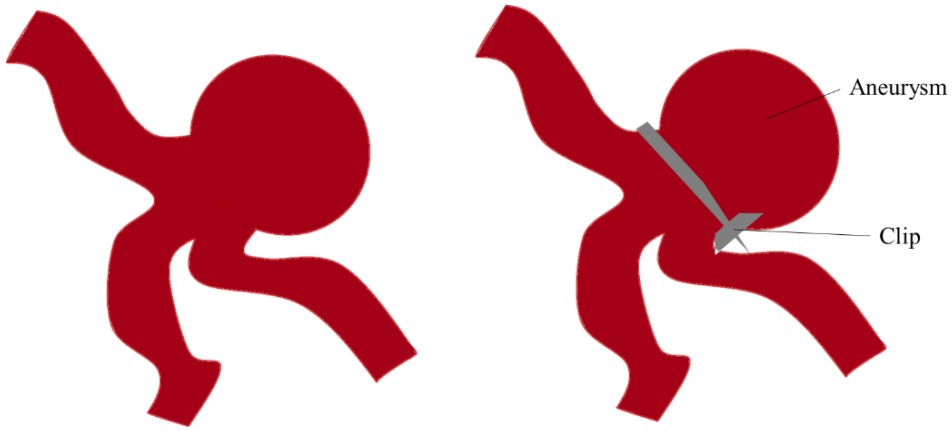

Figure 1-2 Schematic of surgical clipping treatment for aneurysms.

1.4.2 Endovascular coiling

In 1990s, Guglielmi et al. developed the detachable coils system for treating the intracranial aneurysms by combining the techniques of electrothrombosis and endovascular which was named as Guglielmi Detachable Coils (GDC) [66-72].

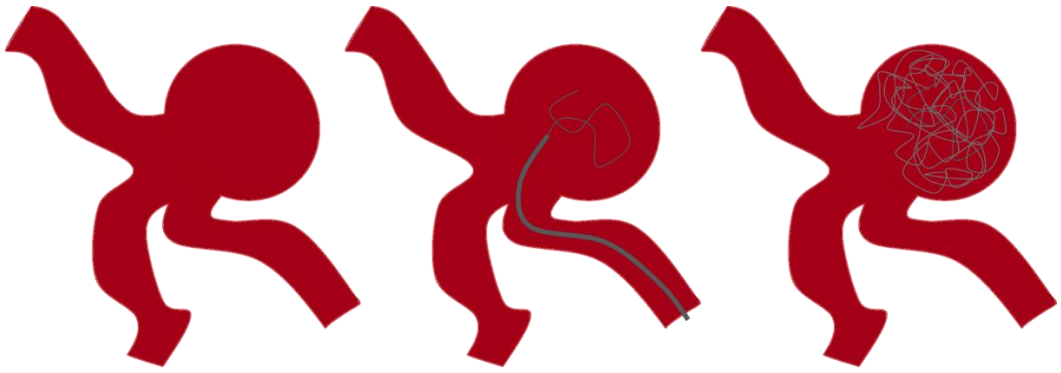

Figure 1-3 Schematic of Guglielmi Detachable Coils treatment for aneurysms.

In the coil embolization procedures as shown in Figure 1-3, coils in the microcatheter were delivered to the location of aneurysm. Small current was used to make

the coil detach from the wire by electrolytic mechanism, then the coil occupied the space of aneurysm with a desired configuration. There are some shortcomings for this approach including the long-time of coil deployment, incomplete occlusion, and no treating ability for large size aneurysm.

1.4.3Porous SMPs

Porous SMPs become a great candidate for the potential treatment of ICAs due to its unique properties mentioned above [47,73,74]. The porous SMPs can be compressed into a small size and put inside the microcatheter. The embolic device can be delivered to the aneurysm location, then porous SMPs can be triggered by thermal stimulus to detach from the microcatheter and recover to the original shape so that the space of aneurysm can be fully occupied, as shown in Figure 1-4).

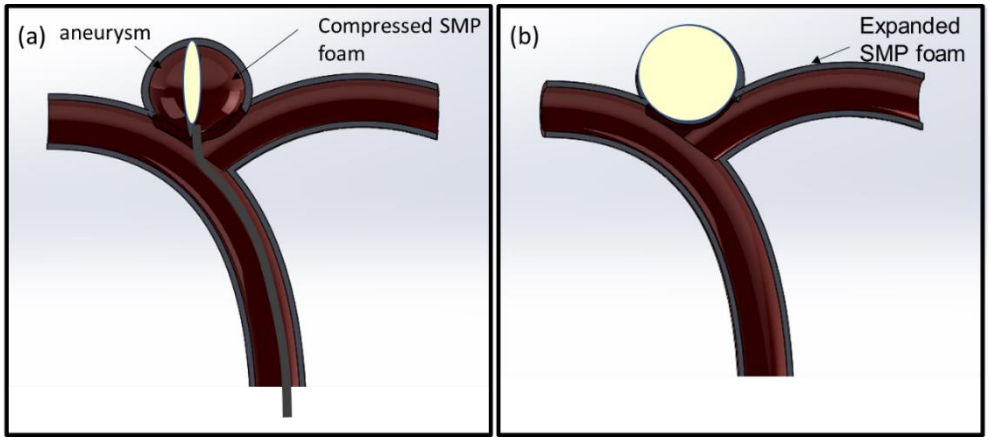

Figure 1-4 Embolization of highly porous SMPs.

Compared to the metal coils, the cost of porous SMPs is much lower and the space occupation is much higher. The glass transition temperature of porous SMPs can be tuned close to human body which is biodegradable and biocompatible.

1.5 CNT/SMP nanocomposites

Although porous SMP is a great potential candidate for ICA treatment, there are some limitations for it including low electrical conductivity, poor mechanical properties, and fatigue susceptibility [75-79]. CNTs are a significant reinforcement for polymer matrix to solve the above problems. The tensile strength and elastic modulus are extremely high and excellent conductivity of CNTs can help SMP triggered by current, making CNT/SMP nanocomposites expand uniformly under the external stimulus [80,81].

Ni et al.[82] investigated the effect of the CNTs under different weight fraction in CNT/SMP nanocomposites. The increasing incorporation of CNTs increased the modulus and yield stress depending strongly on temperature. The shape recoverability was outstanding after multiple cycles of loading. The recovery stress was also improved due to the existence of CNTs compared with pure SMP bulk.

1.6 Thesis objective and outline

The main goal of this thesis is to use the sacrificial template approach and 3D printing technique to fabricate different porous SMP structures including pristine SMP foams, CNT/SMP nanocomposite foams and CNT/SMP nanocomposite scaffolds for the potential treatment of ICAs.

Chapter 1 gives the literature review of fabrication and application of SMPs, the treatments of ICAs and introducing of CNTs in SMP nanocomposites. Chapter 2 discusses the pristine SMP foams fabricated by sacrificial sugar templates. The synthesis process will be detailed and various characterizations including morphologies, mechanical properties,

electrical resistance and shape recovery behavior will be presented. Based on the work of Chapter 2, Chapter 3 introduces the CNT to form the CNT/SMP nanocomposite foams, repeating the same characterization of previous chapter. The protype demonstration of how the CNT/SMP nanocomposite foams occupy the space of the simulated ICAs will be shown. Chapter 4 uses the 3D printing technique to synthesize the CNT/SMP nanocomposite scaffolds. The printing parameters will be optimized, and the scaffolds will be characterized. Chapter 5 summarizes the major work of this thesis and gives the suggestions for future work.

Chapter 2 Synthesis and Characterization of Pristine SMPs

2.1 Introduction

In this chapter, sacrificial sugar template was used to synthesize the pristine porous SMPs. The density, pore size and porosity were characterized by SEM images and physical measurements. Shape recovery behavior of SMP foams were illustrated by direct heat on a hotplate and electrical resistance heating via carbon fiber applied with current. The mechanical performance of SMP foams was tested via failure and cyclic tests under the compression.

2.2 Materials

The SMP foams were synthesized by the following three monomers with the molar ratio of 0.05:0.6:1 which were purchased from Sigma Aldrich: N, N, N', N'-Tetrakis (2-Hydroxypropyl) ethylenediamine (HPED, ≥ 98.0%), Triethanolamine (TEA, ≥ 99.0%), and Hexamethylene diisocyanate (HDI, ≥ 99.0%). Pure cane sugar particles (Florida Crystals Inc.) purchased from local store were used as template to synthesize porous SMP foams. All materials were used as received.

2.3 Synthesis of solid and porous SMPs

The high-speed shear mixer was used to mix the HDI, HPED and TEA for 5 to 6 min after the weight of each was measured. Then the mixed polymer solution was poured into the dog-bone mold following the standard of ASTM D638 Type V with a dimension of 45 mm by 8 mm by 1 mm. Bubbles were removed by degassing for three times in a vacuum oven under the protection of nitrogen environment. The curing procedures were followings: materials were kept at room temperature for 1h, then heated up to 130 °C with a ramp of 9.6 °C per hour, lastly held at 130 °C for 1h. After natural cooling to room temperature, fully cured solid SMPs were token out from the

molds. All the SMP samples were sealed in vacuum bags and stored in a vacuum tank so that no moisture would contaminate the SMPs for later characterizations.

SMP foams were synthesized using a sacrificial sugar template, as shown in Figure 2-1. Sugar particles were sprayed with a slight amount of water to improve interfacial bonding and make the sugar particles to form the cubic configurations in molds. Then the sugar particles in the silicon rubber mold were compressed at 30kN load for 10 minutes. The size of sugar particles was about 500μm which was measured by SEM. After compression, the mold was put into oven for 1h at 130 ℃ to remove the moisture and form interconnected sugar templates.

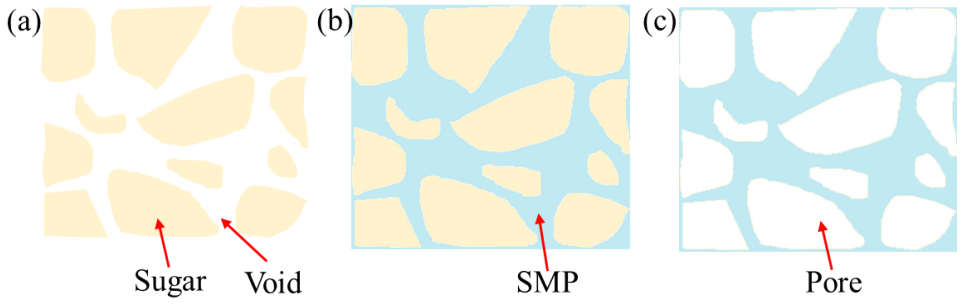

Figure 2-1 Schematic of sacrificial sugar template method for fabrication of porous SMP foam: (a) Sugar template; (b) Sugar template after SMP infiltration; (c) SMP foam after dissolving sugar particles.

SMP solution prepared by the three monomers with the process mentioned above was poured onto the sugar templates in a dish. Then the dish was put in a vacuum container which later was put inside a freezer at -5 ℃ for 24h. The low temperature slowed down the reaction rate of SMP solution and extended the infiltrating time of SMP solution into the sugar templates. The vacuum helped accelerate the infiltrating compared with no vacuum procedure. After infiltrating, the sugar particles/SMP composites were cured with the process mentioned above for solid SMPs. Then the fully cured sugar particles/SMP composites were put in a beaker full of Di water. The beaker was kept in a bath sonication for 12h to dissolve all the sugar and the water was replaced

every 3h. After the sugar was dissolved, porous SMPs were left and then put in a vacuum oven at 40 °C for 24h to remove all the moisture.

2.4 Characterizations

Shape recovery behavior of SMP foams was investigated by the direct heating method which used a hotplate to heat the foam at 70 °C for 2 min to memorize the shape after a quick cooling. Then the recovered shape of SMP foam was obtained when the foam was put on the hotplate again at 70 °C.

SEM was used to characterize the microstructure, pore size and porosity of SMP foams. The surface conductivity of SMP foams was improved by sputter coating which prevented the charging in the SEM imaging process. The top surface and cross-section in the middle of SMP foams were chosen for SEM images. Lower magnification at about 50 to 100 which could observe enough pores in SEM images was set. Based on the SEM images, the average pore size of SMP foams was analyzed by Image J software.

The porosity of the SMP foams was calculated using Eq.(1) shown below.

$$Porosity = 1 - \frac{\rho_{porous\ SMP}}{\rho_{solid\ SMP}} \quad (1)$$

where $\rho_{porous\ SMP}$ was the density of porous SMP foams, obtained by the mass of porous SMPs divided by the volume of porous SMPs. The $\rho_{solid\ SMP}$ was the density of solid SMPs, calculated by dividing mass of solid SMPs to volume of solid SMPs. The masses of both solid and porous SMP samples were measured using a digital scale and the volume was calculated by the dimensions of the cubes. In order to improve the accuracy and repeatability, ten samples were measured and averaged.

The mechanical properties of SMP foams were tested by the Instron 5969 universal testing system with a thermal chamber, as indicated in Figure 2-2 (b). SMP foam cubes with a dimension of 10mm by 10mm by 10mm were compressed to the strain failure at room temperature. Then the 40% of failure strain (~90%) was set to conduct the cyclic compression test for 10 cycles. The cyclic testing was done at room temperature, T_g (39 °C) and T_g+10 (49 °C). The rate of all compression testing was 2mm/min. Before the compression testing, all SMP foam cubes were preheated in the thermal chamber for 30 min to reduce the heat effect.

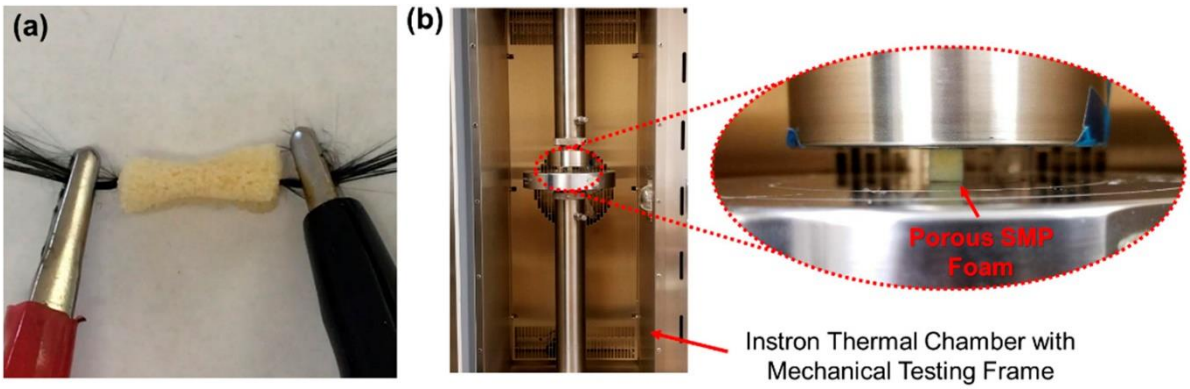

Figure 2-2 (a) Illustration of electrically-heated activation of shape recovery of SMP foams using carbon fibers. (2) Setup of mechanical test of SMP foams in thermal chamber.

Carbon fibers were used to simulate the deployment and expansion of SMP foams due to the electrical heating property. A bundle of carbon fibers was inserted through the middle of SMP foams with the dimension of 10mm by 10mm by 15mm using a needle, as shown in Figure 2-2 (a). The SMP foam was heated to 50 °C, then manually compressed into small volume, and quickly cooled at room temperature to memorize the temporary shape. The buddle of carbon fibers was applied with 0.5 1.0, 1.5 and 2.0 amperes to generate the heat which triggered the SMP foam to return to the original shape. An infrared (IR) camera was used to measure the surface temperature every 10s to demonstrate the temperature field of heated SMP foams.

2.5 Shape recovery of SMP foams

As demonstrated in Figure 2-3, the temporarily memorized shape of SMP foam was shown in the image at 0s which was compress into less than the half volume of original shape. When the SMP foam was put on the heat hotplate, the shape of SMP foam gradually expanded. It took about 50s for the SMP foam to recover to the original shape.

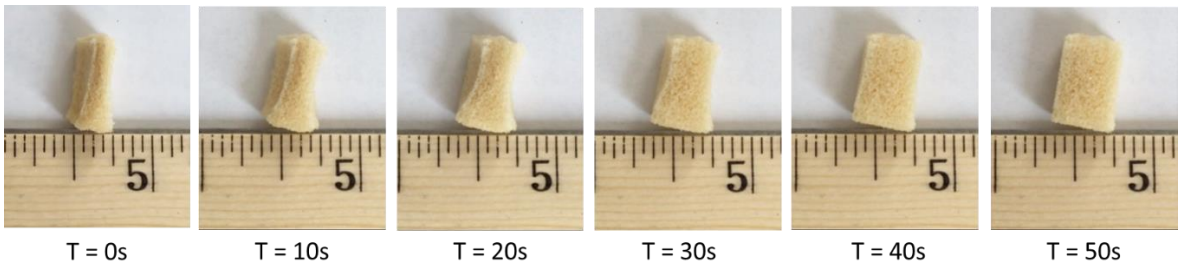

Figure 2-3 Illustration of expansion and shape recovery of SMP foam responding to the heat generate by a hotplate.

2.6 Microstructure analysis

Pore size of SMP foams was studied by SEM images as shown in Figure 2-4. The average size of pores is around 480um based on the measurement on SEM images. There were no sugar particles left in the SEM images which proved that the dissolving of sugar particles was completed and effective.

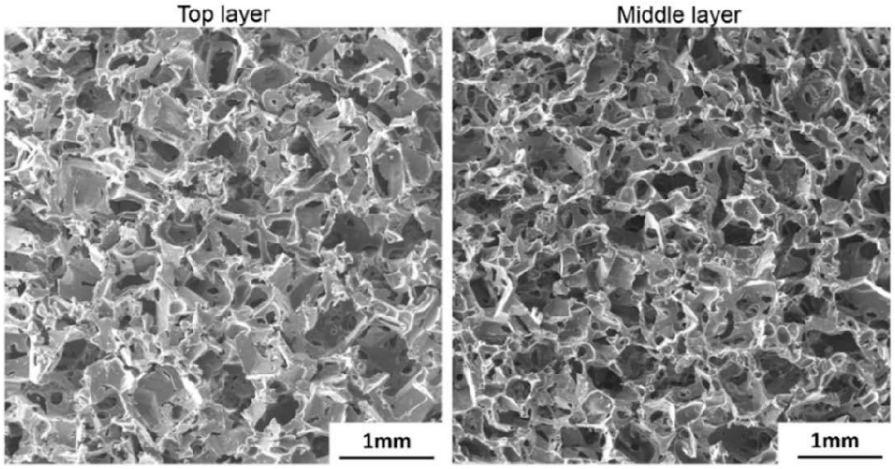

Figure 2-4 SEM images of top later and middle layer of SMP foam.

The average densities of solid and porous SMPs were 1.172 g/cm^3 and 0.168 g/cm^3, respectively. Based on the equation in characterization part, the porosity of SMP foams was calculated which was 85.7%. This high porosity will make the SMP foam have high compressive capability when the temperature was above the T_g, which make it suitable for the different size of ICAs as embolic devices.

2.7 Compression testing

SMP foams were compressed to the failure fracture when the strain was near 90% that was considered as failure strain at room temperature. For conducting the cyclic tests, a 35% compressive strain which was about 40% of failure strain was used. Figure 2-5 (a) showed the one cycle of loading and unloading process of SMP foam in cyclic compressive test which leaded to the plastic deformation. The elastic modulus of SMP foam at room temperature was 2.7 ± 0.12 MPa. When the temperature increased to the T_g or high, The SMP foam was softened greatly with the modulus of 0.23 ± 0.017MPa and 0.18 ± 0.012 MPa when the temperature was at 39 °C and 49 °C. When the SMP foam was deployed to the location of ICAs, the softened SMP foam could reduce the rupture risk of vessel.

Besides, the strain recovery was evaluated by the cyclic compressive test at T_g and T_g + 10 °C as shown Figure 2-5 (b) and (c). There was an initial hysteresis when the foam was loaded and unloaded which may owe to the relaxation of polymers, residual stress and re-arrangement of polymer chains. The hysteresis was significant after the first cycle of loading and unloading. The maximum stress was reduced for each cycle as the SMP foam was continuously softened by the compressive force. The tailored mechanical properties and behaviors can be used to design the device of SMP foams for potential treatment of ICAs.

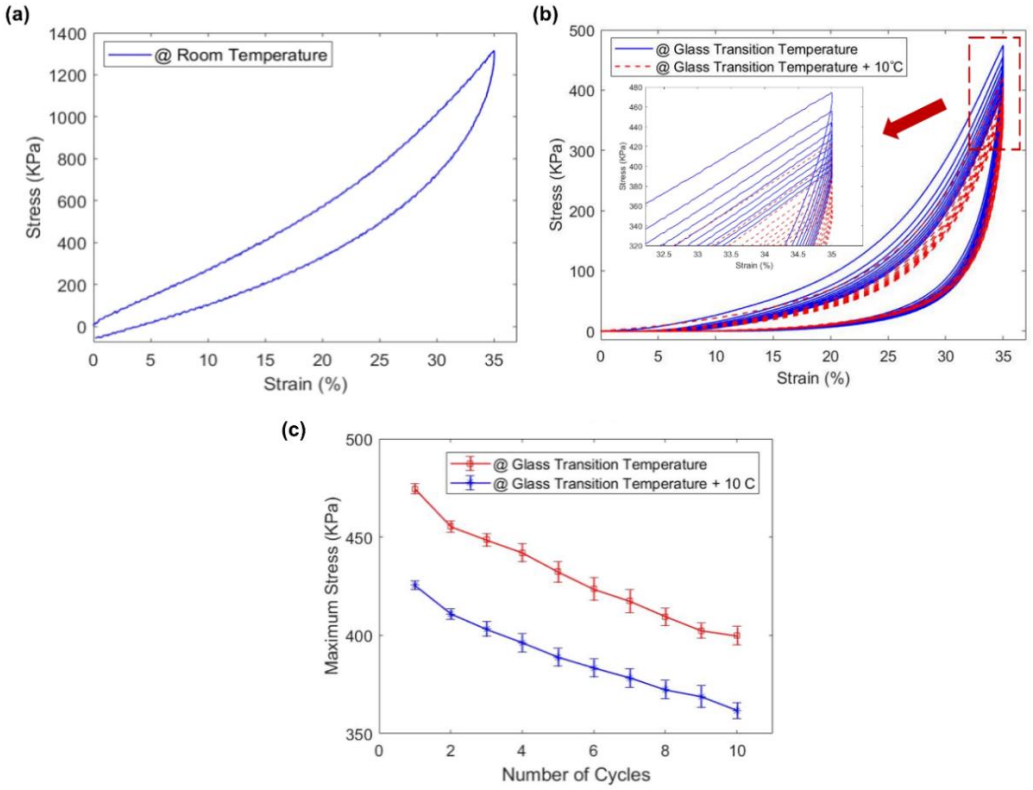

Figure 2-5 Compression tests: (a) loading/unloading of one cylce in cyclic testing at room temperature, (b) cyclic testing of SMP foam at T_g and T_g+10 °C, (c) Maxmimum stress of each cylcle in cyclic testing at T_g and T_g+10 °C.

2.8 Electrical resistance heating

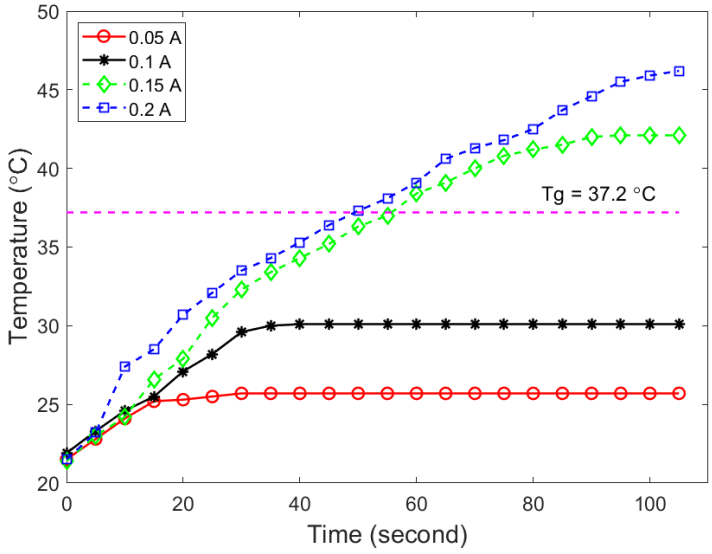

Figure 2-6 Surface temperature of the SMP foams depent on time when current was applied.

As carbon fibers works as a media to generate heat to trigger the shape recovery of SMP foams, the relation between applied current and equilibrium temperature of SMP foam is very important, which was shown in Figure 2-6. When the carbon fibers were applied with current of 0.05 A and 0.1 A, the temperatures of SMP foams did not reach over the T_g, which were only 25.7 °C and 31.3 °C. Even low current is safe for human, it will not generate enough heat to recover the shape of SMP foam, so high currents were applied. The temperatures of SMP foams were equilibrated at 43.2 °C and 47.8 °C when the applied currents were 0.15A and 0.2A. When human vessel was shortly exposed to temperature over 45 °C in less than 5 min, it will be permanently damaged [83,84], so 0.15A current is the optimal result for the potential bio-application.

2.9 Shape recovery behavior

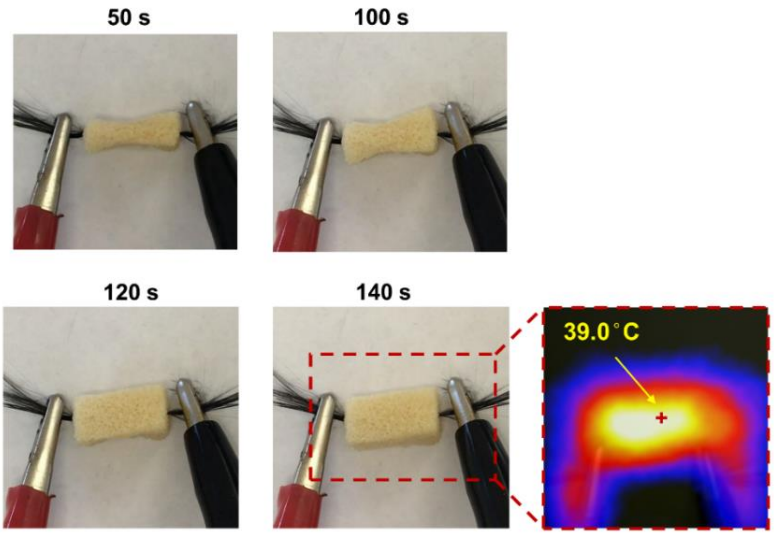

Figure 2-7 Illustration of shape recovery of SMP foam when 0.15A current was applied on carbon fibers and of tempearture field of SMP foam at 140s using an IR camera.

The process of shape recovery and expansion of SMP foam was indicated in Figure 2-7, when the SMP foam was triggered by the heat generated by carbon fiber which was applied with current of 0.15A. After 140s, the original shape of SMP foam was achieved and temperature of foam was 39.0 °C with the result of an IR camera. The successful shape recovery of SMP foam

under 1.5 A current resulting in the temperature at 39 °C which was safe to human made the SMP deployment possible for potential ICA treatment.

Chapter 3 Development of CNT Reinforced SMP Nanocomposite Foams

3.1 Introduction

CNT/SMP nanocomposite foams were synthesized via a sacrificial template technique, and the density was controlled by selecting the various sizes of sugar particles and adding different concentrations of CNTs. The densities of CNT/SMP nanocomposite foams were studied, and porosities of foams were calculated. The mechanical properties of CNT/SMP nanocomposite foams were characterized at room temperature, T_g, T_g+5 °C, and T_g+10 °C by uniaxial compressive loading. The electrical resistivity of CNT/SMP nanocomposite foams at room temperature was investigated. Joule-heating was applied for evaluating the shape recovery behavior of CNT/SMP nanocomposite foams. Finally, a potential design for treating ICAs using CNT/SMP nanocomposite foams was demonstrated.

3.2 Materials

All chemicals were used as received. Three monomers: (i) Hexamethylene diisocyanate (HDI, ≥ 99.0%, Sigma-Aldrich), (ii) N, N, N', N'-tetrakis (hydroxypropyl) ethylenediamine (HPED, ≥ 98.0%, Sigma-Aldrich), (iii) Triethanolamine (TEA, ≥ 99.0%, Sigma-Aldrich) were utilized to synthesize the SMP solution for later composite fabrication. The molar ratio of HDI, HPED, and TEA was 1:0.05:0.6 [85]. Multi-walled CNTs (>95% carbon basis) with a density of 2.1 g/cm^3 and a diameter of 50-90 nm were purchased from Sigma-Aldrich to improve the electrical conductivity of SMP nanocomposites. Ethanol (95%), a non-toxic organic solvent, was selected to disperse CNTs.

3.3 Synthesis of CNT/SMP nanocomposite foams

The porous CNT/SMP nanocomposites were synthesized via a sacrificial template, and the synthesis procedure was shown in Figure 3-1. Pre-calculated weight of CNTs were added into 60 ml ethanol and dispersed by probe sonication at 28% amplitude in pulse mode with 5 seconds on and 2 seconds off for 10 minutes. Then sugar particles were mixed with the dispersed solution by glass rod about 10 minutes after dispersion.

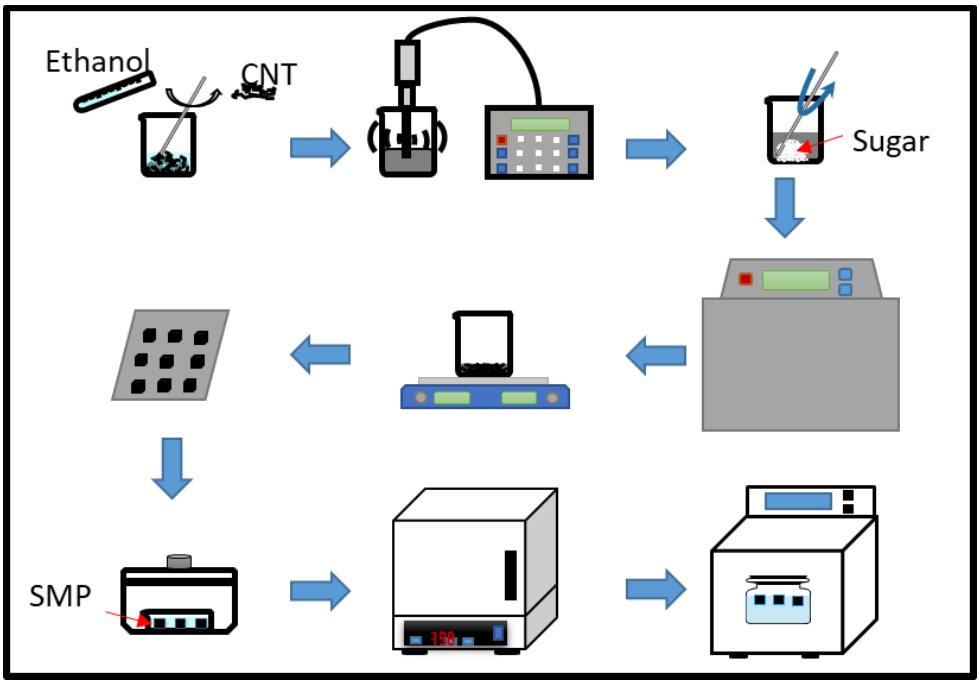

Figure 3-1 Synthesis procedures of CNT/SMP nanocomposite foams.

The beaker contained with the mixed sugar/CNT solution was put into bath sonicator for 24 hours to fully coat the sugar particles with CNTs. After sonication, the beaker was transferred to the hotplate with heating and stirring to remove the solvent for 12h. The temperature was 120 °C and stirring speed was 200rmp. The sugar particles coated with CNTs were sprayed with a slight amount of water to improve interfacial bonding and make the sugar particles to form the cubic configurations in molds. Then the sugar particles in the silicon rubber mold were compressed

at 30kN load for 10 minutes. After compression, the mold was put into oven for 1h at 130 ℃ to remove the moisture and form interconnected sugar template.

SMP solution prepared by the three monomers was poured onto the sugar templates in a dish. Then the dish was put in a vacuum container which later was put inside a freezer at -5 ℃ for 24h. The low temperature slowed down the reaction rate of SMP solution and extended the infiltrating time of SMP solution into the sugar templates. The vacuum helped accelerate the infiltrating compared with no vacuum procedure. After infiltrating, the sugar particles/CNT/SMP composites were cured in oven with temperature from room temperature to 130 ℃ at a ramp of 10 ℃ per hour. Then the fully cured sugar particles/CNT/SMP composites were put in a beaker full of DI water. The beaker was kept in a bath sonication for 24h to dissolve all the sugar and the water was replaced every 3h. After the sugar was dissolved, porous CNT/SMP nanocomposites were left, then put in a vacuum oven at 40 ℃ for 36h to eliminate all the water in the foams. All the foams were stored in a vacuum container for later tests.

Templates were fabricated with sugar particles of small, medium, and large size with CNT concentration of 1.25%. CNTs with concentrations of 0.5%, 0.75%, 1.00% and 1.25% in ethanal combined with sugar particles of small size were prepared for the templates.

3.4 Characterizations

The porosity of the SMP foams was calculated using Eq.(2) shown below.

$$Porosity = 1 - \frac{\rho_{porous\ SMP}}{\rho_{solid\ SMP}} \tag{2}$$

where $\rho_{porous\ SMP}$ was the density of porous CNT/SMP foams, obtained by the mass of porous CNT/SMP nanocomposites divided by the volume of porous CNT/SMP nanocomposites. The $\rho_{solid\ SMP}$ was the density of solid SMPs, calculated by dividing mass of solid SMPs to

volume of solid SMPs. The masses of both solid and porous SMP samples were measured using a digital scale and the volume was calculated by the dimensions of the cubes. In order to improve the accuracy and repeatability, ten samples were measured and averaged.

The mechanical properties of CNT/SMP nanocomposite foams were tested by the Instron 5969 universal testing system with a thermal chamber, as indicated in Figure 2-2 (b). Foam cubes of CNT/SMP nanocomposites with a dimension of 8mm by 8mm by 12mm were compressed to the strain failure at room temperature. Then the 50% of failure strain (~70%) was set to conduct the cyclic compression test for 10 cycles. The cyclic testing was done at room temperature, T_g (39 °C) and T_g+10 (49 °C). The rate of all compression testing was 2mm/min. Before the compression testing, all CNT/SMP foam cubes were preheated in the thermal chamber for 30 min to reduce the heat effect.

For measuring the electrical resistivity, CNT/SMP nanocomposite foams were dried before usage. A slight amount a silver Epoxy glue was put on the top and bottom surface of sample, then copper tape was attached on the surface with glue. The samples were put in room temperature for 24 hours for drying the glue. The resistivity of SMP/CNT composite foam with different CNT weight concentration was measured using electric multimeter at room temperature.

Carbon fibers were used to simulate the deployment and expansion of CNT/SMP nanocomposite foams due to the electrical heating property. A bundle of carbon fibers was inserted through the middle of CNT/SMP foams using a needle. The CNT/SMP foam was heated to 50 °C, then manually compressed into small volume, and quickly cooled at room temperature to memorize the temporary shape. The buddle of carbon fibers was applied with 0.5 1.0, 1.5 and 2.0 amperes to generate the heat which triggered the CNT/SMP foam to return to the original shape.

An infrared (IR) camera was used to measure the surface temperature every 5s to demonstrate the temperature field of heated CNT/SMP foams.

3.5 Density of CNT/SMP nanocomposite foams

The densities of CNT/SMP nanocomposite foams synthesized by various concentrations of CNTs and different size of sugar particles were shown in Figure 3-2. The density of samples increased with the increasing amount of CNTs, ranging from 0.3663 to 0.4465 g/cm^3. The density got larger since more CNTs were coated on the sugar particles in the sonication step leading to more CNTs in polymer matrix.

For different sugar size-based foams with CNT concentration of 1.25 wt. %, the densities of each size were 0.4665 g/cm^3, 0.3520 g/cm^3, and 0.3380 g/cm^3, respectively. As the volume of all template cube was the same, sugar particles of large size resulted in more dissolving which leaded to the lower density.

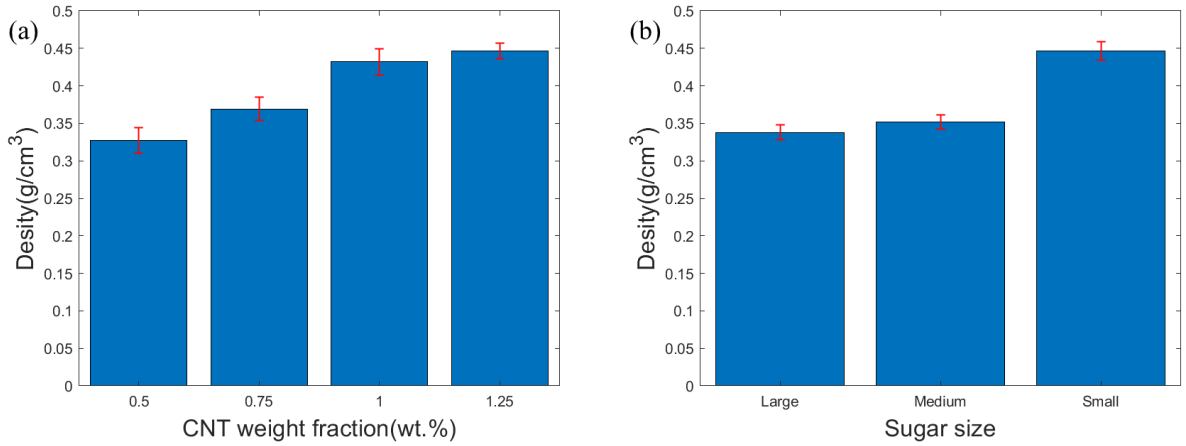

Figure 3-2 Densities of CNT/SMP nanocomposite foams: (a) effect of CNTs, (b) effect of sugar size.

The porosities of CNT/SMP nanocomposite foams were calculated by Eq. (2). The average density of neat SMPs is 1.172 g/cm^3, so the estimated porosities of the porous CNT/SMP nanocomposites with CNT concentration of 0.5-1.25 wt.% were 68.7%, 63.1%, 62.0%, and 61.9%,

respectively. The estimated porosities of CNT/SMP nanocomposite foams fabricated with sugar particles of small, medium, and large size with 1.25 wt.% CNT concentration were 61.9%, 69.9%, and 71.2%.

It is expected that large volume expansion will be achieved by the low density and high porosity of CNT/SMP nanocomposite foams[86,87], but the mechanical properties and conductivity of CNT/SMP nanocomposite foam should be considered at the same time so that the design of potential embolic devices for treating ICAs may be realized.

3.6 Failure test

For uniaxial compressive failure test at room temperature, a clear fracture appeared when the foam samples were compressed to near 70% strain. The result of failure test for CNT/SMP nanocomposite foams fabricated by sugar templates of small, media and large particles was shown in Figure 3-3. The maximum stress of foam samples made by small sugar particles was larger than the medium and large ones, due to the differences of densities caused by the dissolving of sugar particles.

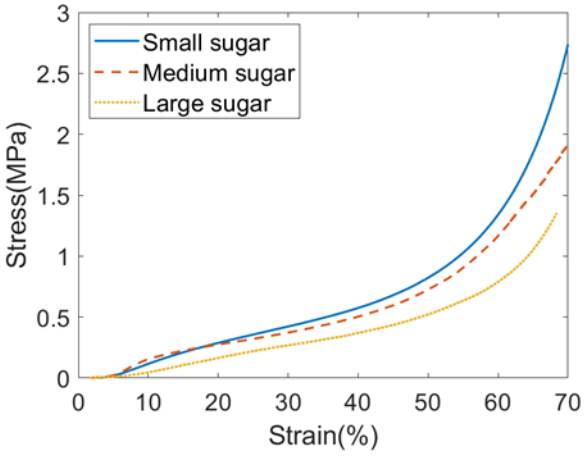

Figure 3-3 Faliure testing of CNT/SMP nanocomposite foams fabricated by different size of sugar particels with CNT concentration of 1.25 wt. %.

3.7 Cyclic test

At room temperature, the elastic modulus of CNT/SMP nanocomposite foams with CNT concentration of 0.5 wt.% was 58.23 MPa. The CNT/SMP nanocomposite foams became soft when applied mechanical test at temperature of its T_g or higher. The elastic moduli of the same CNT concentration foam samples obtained from Instron were 5.37 MPa, 4.66 MPa, and 3.61 MPa at T_g, T_g+5 °C, and T_g+10 °C, respectively. The elastic modulus of the CNT/SMP nanocomposite foams dropped by about 10 times when the temperature raised to its T_g or higher. The softened samples would have a low risk of failure for the embolization treatment of aneurysm because of the mechanical properties mentioned above.

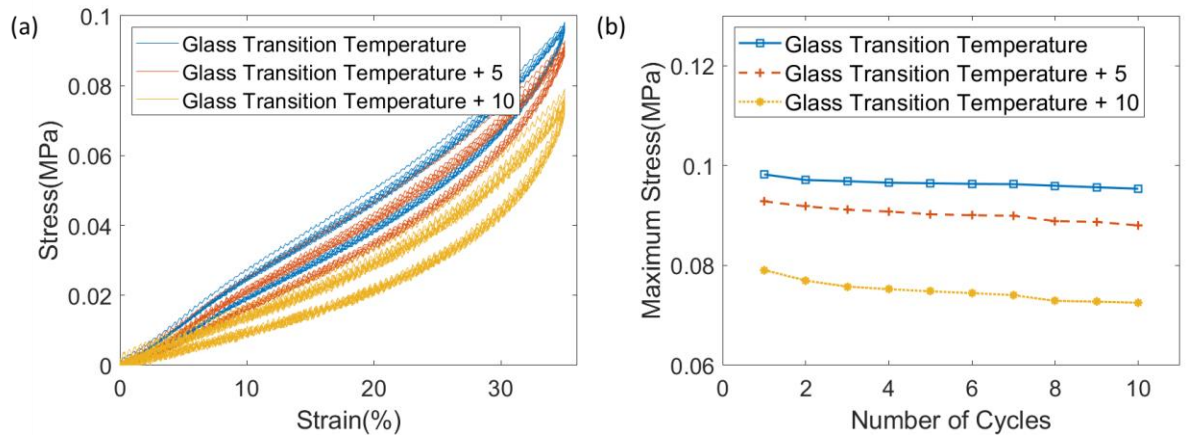

Figure 3-4 Mechanical characterizations of CNT/SMP nanocomposite foams under cyclic compressive loading conditions: (a) mechanical response of the CNT/SMP nanocomposite foams at T_g, T_g+5°C, and T_g+10°C; (b) mechanical response of each cycle at T_g, T_g+5°C, and T_g+10°C.

Cyclic compressive testing was applied to investigate the extension of strain recovery for application of CNT/SMP nanocomposite foams. The cyclic compression testing was applied on the samples at T_g, T_g+5 °C, and T_g+10 °C, as shown in Figure 3-4. The initial hysteresis phenomenon appeared in the loading and unloading cycle, which could be associated with residual stress, material relaxation, and re-arrangement of dangling chains in the foam samples [88]. The hysteresis which appeared in each loading and unloading, reduced the maximum stress at each

cyclic compressive loading, which was shown in Figure 3-4(a). For 10 cycle compression testing, and the maximum stress in 10th cycle was about 92% of the value in the first cycle (see Figure 3-4 (b)). From Figure 3-4 (b), it was found that the slope of maximum stress tended to be flat after 6th cycle at T_g, so it seemed that the maximum stress did not change much after 6th cycle, resulting an optimal recovery behavior with low degradation. The low degradation made CNT/SMP nanocomposite foams a potential candidate for ICA treatment.

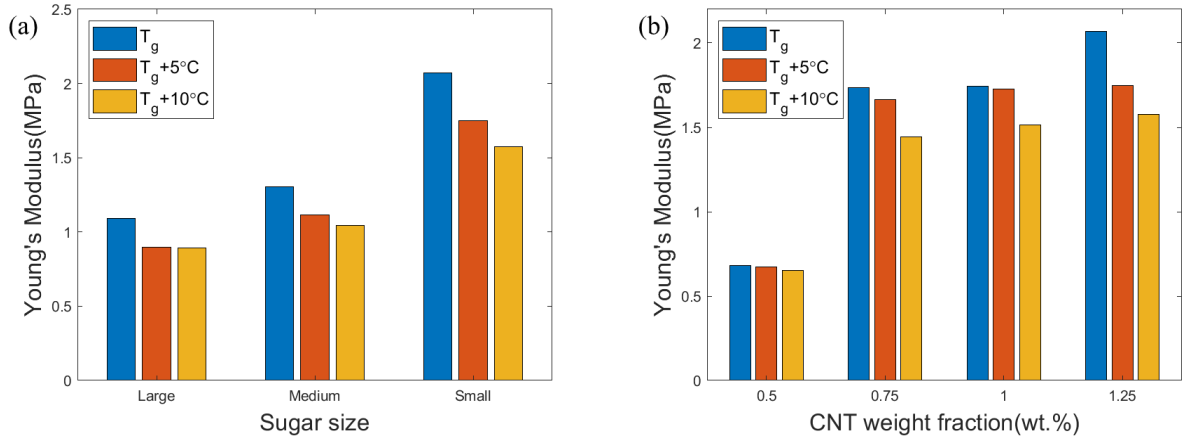

Figure 3-5 Modulus of CNT/SMP nanocomposite foams: (a) effect of sugar size, (b) effect of CNT concentration.

As shown in Figure 3-5 (a), Young's modulus of CNT/SMP nanocomposite foams made of various sugar particle sizes, decreased when the temperature increased from T_g to T_g+10 °C, since the foams became much more soft when they were applied with higher temperature. The same results were found for the CNT/SMP nanocomposite foams fabricated with different CNT concentration, which was shown in Figure 3-5 (b). The improved modulus was due to the mechanical properties improved by increasing concentration of CNTs which enhanced pore structure and stiffness [89].

3.8 Electrical resistivity

The top and bottom surface of CNT/SMP nanocomposite foams with a dimension of 10mm by 10mm by 8mm) were glued with copper tape by silver epoxy adhesive. The resistance of the foams was measured by a digital multimeter, and the electrical resistivity was calculated by

$$\rho = \frac{RA}{l} \tag{3}$$

where R is the resistance of the foams, A is the cross-sectional area of the foams, and l was is length between two copper plates (showed in Figure 3-6).

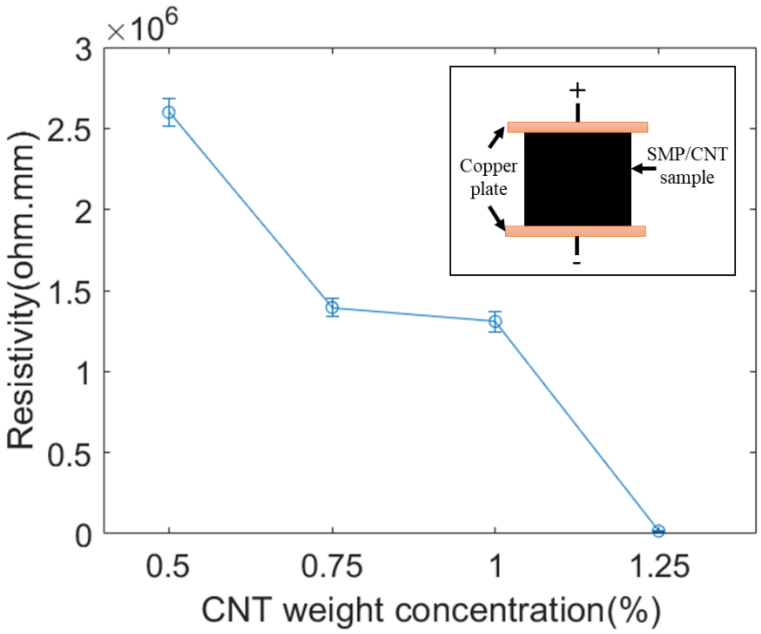

Figure 3-6 Electrical resistivity of CNT/SMP nanocomposite foams under various CNT concentrations.

As shown in Figure 3-6, the electrical resistivities of CNT/SMP nanocomposite foams were 2.6 * 10^6 Ω·mm, 1.4 * 10^6 Ω·mm, 1.3 *10^6 Ω·mm, and 1.6*10^4 Ω·mm, when CNT concentration was 0.5 wt.%, 0.75 wt.%, 1.0 wt.%, and 1.25 wt.% , respectively. When the CNT concentration less than 1 wt.%, the CNTs in the foams could not form conductive path due to their separation, resulting the high resistivity up to 10^6 Ω·mm. However, when CNT concentration was more than

1 wt.%, the CNTs were more likely to agglomerate with each other, forming a conductive network. As a result, the resistivity of CNT/SMP nanocomposite foams of 1.25 wt.% CNTs sharply lowered down to 10^4 Ω·mm directly, becoming conductive instantly. The sharp decrease of resistivity was due to the percolation threshold [90,91].

3.9 Electrical resistance heating

The surface temperature of CNT/SMP nanocomposite foams heated by the bundle of carbon fibers which was applied with different currents were shown in Figure 3-7. The applied DC current was 0.05A, 0.1A, 0.15A and 0.20A.

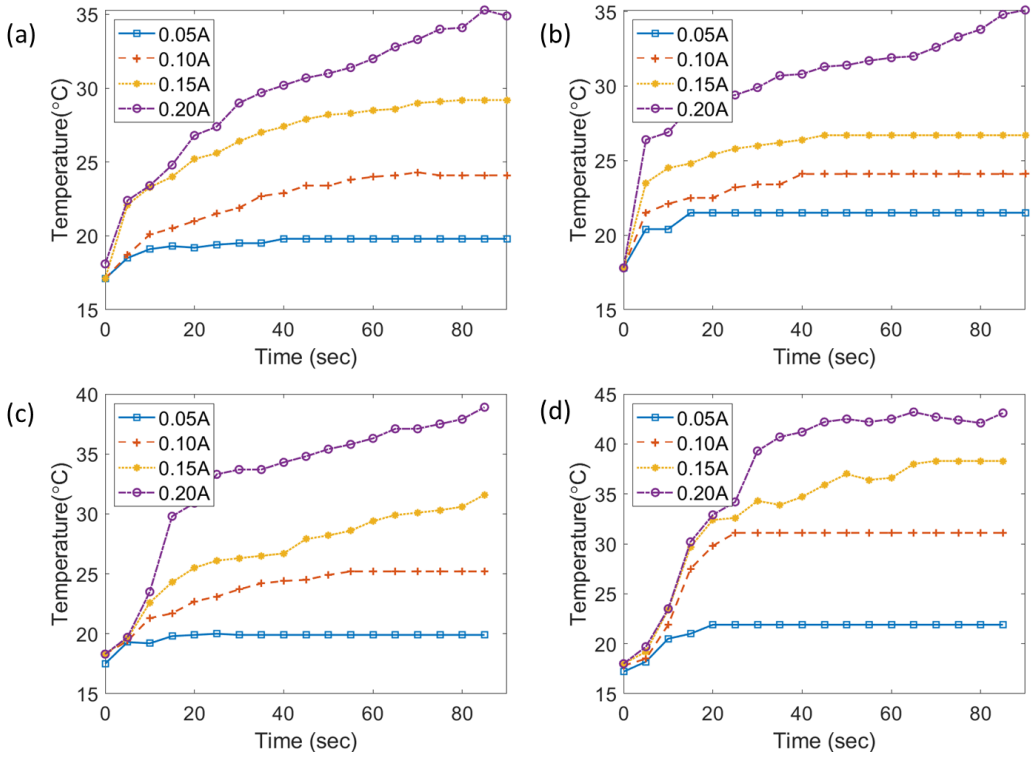

Figure 3-7 Thermal results: (a) 0.5 wt.% CNT/ SMP foam under current ranges from 0.05A to 0.20A, (b) 0.75 wt.% CNT/SMP foam under current ranges from 0.05A to 0.20A, (c) 1.0 wt.% CNT/SMP foam under current ranges from 0.05A to 0.20A, (d)1.25 wt.% CNT/SMP foam under current ranges from 0.05A to 0.20A.

For the foams of lower CNT concentrations, the surface temperature could not rise to its T_g when applied current ranging from 0.05 to 0.2A, which was illustrated in Figure 3-7 (a) and (b).

It was clearly observed that the surface temperature increased quickly once the larger DC current was applied. As shown in Figure 3-7 (a), in 20 seconds, the surface temperature of CNT/SMP nanocomposite foam of 0.5 wt. % CNTs rose about 10°C when applied 0.2 A current, while the temperature rose 8 °C, 5 °C and 2 °C when the foam was applied with current of 0.15A, 0.10A, and 0.05A, respectively. The same phenomenon can be seen in Figure 3-7 (b) to (d).

Besides, the CNT/SMP nanocomposite foam with higher concentration of CNTs, the surface temperature increased much faster. As depicted in Figure 3-7 (b), in 20 seconds, the surface temperature of foam sample of 0.75 wt.% CNTs rose about 12 °C, 9 °C, 6 °C, and 3 °C, at current of 0.2 A, 0.15A, 0.1A, and 0.05A, respectively.

The results indicated that higher CNT concentration in nanocomposites should be employed if the rapid deployment of SMP nanocomposites is required for the surgical applications. However, appropriate DC current should be applied during the deployment due to the potential overheating of SMPs.

3.10 Shape recovery behavior

Once the DC current was applied, the temperature of the CNT/SMP nanocomposite foams increased quickly from ambient temperature up to its T_g, and the shape recovery started, as shown in Figure 3-8 (a)-(c). The compressed nanocomposite sample was able to fully recover to its original shape in about 80 seconds, as shown in Figure 3-8 (c). The temperature of the compressed foam was about 18 °C before applied with current, and the surface temperature reached to 41.3 °C when the foam recovered to its original shape. The shape recovery time of CNT/SMP nanocomposite foams was shorter than that of pristine SMP foams, which was 140 seconds in chapter 2.

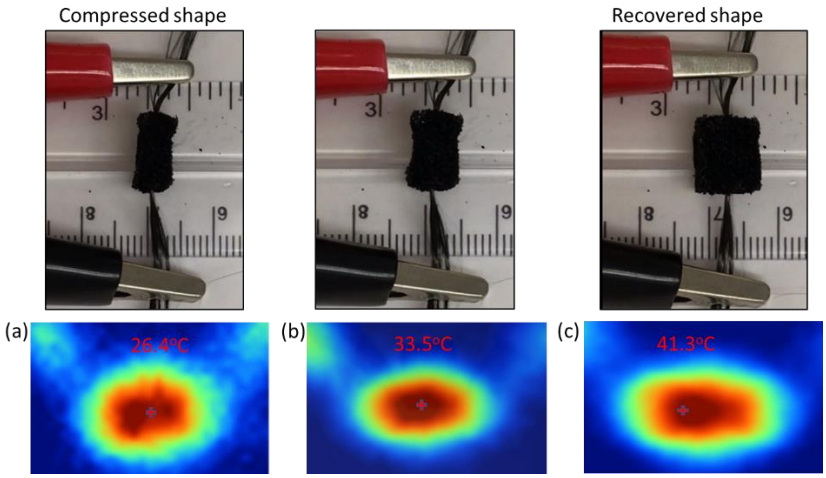

Figure 3-8 Shape recovery of a compressed CNT/SMP nanocomposite using Joule-heating method.

3.11 Demonstration of potential bio-application

The long-term goal of this work is to develop a new biomedical device that can be used to treat ICAs and provide an effective surgical method for optimal patient recovery outcomes. Therefore, a proof-of-concept demonstration of ICA fulfillment was carried out. As shown in Figure 3-9, the compressed CNT/SMP nanocomposite foam was transferred into the aneurysm site via a catheter, and the compressed foam recovered to fill the aneurysm site completely when applied a slight amount of DC current.

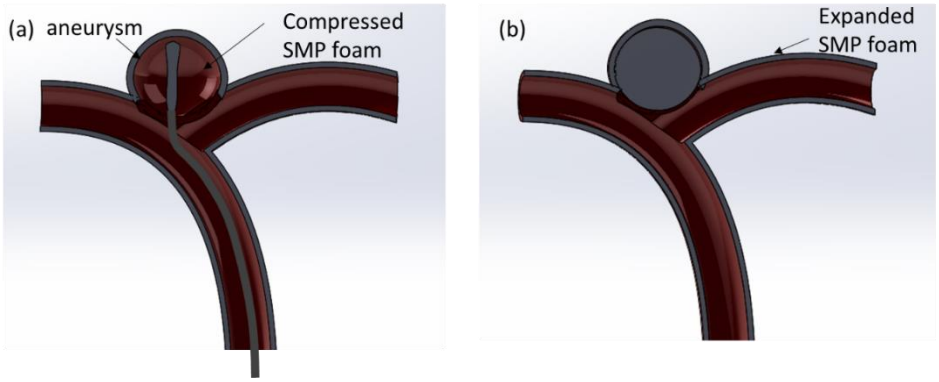

Figure 3-9 Schematic of embolization of intracranial aneurysm using proposed SMP based nanocomposites.

A transparent aneurysm model was manufactured and a piece of compressed CNT/SMP ball was deployed to fill the aneurysm using Joule-heating method. The concept of potential

embolization of intracranial aneurysm using CNT/SMP nanocomposite foams was shown in Figure 3-10.

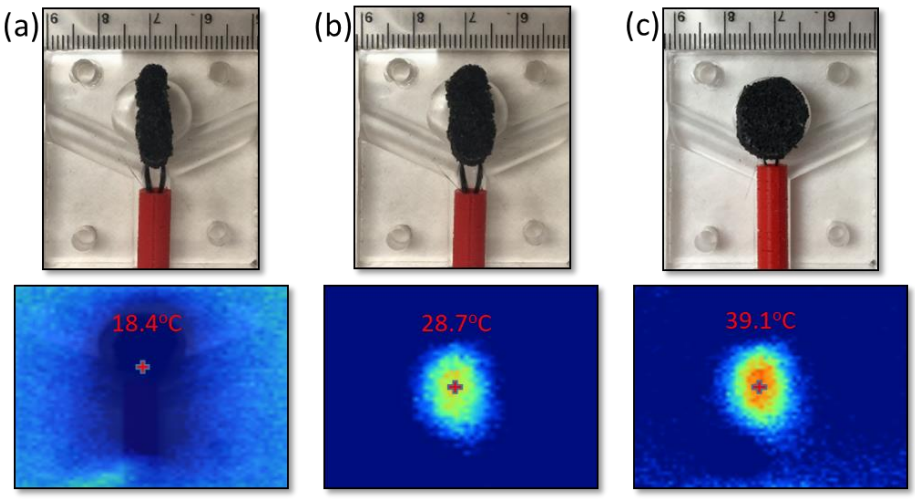

Figure 3-10 Experimental demonstration of embolization of ICA using highly porous SMP/CNT composite foam.

A DC current of 0.15A was employed during the demonstration. The compressed CNT/SMP nanocomposite foam was inserted in a 3D printed red tube, simulating the catheter used to deploy potential biomedical devices for ICA treatment. Once the plastic tube was placed in front of the aneurysm, the compressed CNT/SMP nanocomposite foam was delivered to the aneurysm site. The 0.15A DC current was able to quickly heat the nanocomposite foam above its T_g, thus, the compressed CNT/SMP nanocomposite foam was able to be fully developed in 80 seconds. The surface temperature of the foam was measured by IR camera during the experiment. The maximum surface temperature of 39.1 °C was measured. Since the maximum surface temperature of SMP nanocomposite was below 43 °C, the heat generated by the CNT/SMP nanocomposite foam during deployment was considered to be biologically safe and should not cause any potential damage to the tissue within and around the treated aneurysm.

Chapter 4 3D Printed CNT/SMP Nanocomposites

4.1 Introduction

CNT/SMP nanocomposites were fabricated by 3D printing technique. Different weight fractions of CNTs were added to prepare for the printing ink. The printing parameters including weight fractions of CNTs, infill rate and printing speed were optimized. Mechanical, thermal and electrical properties of 3D printed CNT/SMP nanocomposites were characterized. Shape recovery behavior of 3D printed nanocomposite beams were investigated by electrical resistance heating and direct heating.

4.2 Materials

All chemicals were used as received. Three monomers: (i) Hexamethylene diisocyanate (HDI, ≥ 99.0%, Sigma-Aldrich), (ii) N, N, N', N'-tetrakis (hydroxypropyl) ethylenediamine (HPED, ≥ 98.0%, Sigma-Aldrich), (iii) Triethanolamine (TEA, ≥ 99.0%, Sigma-Aldrich) were utilized to synthesize the SMP solution for later composite fabrication. The molar ratio of HDI, HPED, and TEA was 1:0.05:0.6. Multi-walled CNTs (>95% carbon basis) with a density of 2.1 g/cm^3 and a diameter of 50-90 nm were purchased from Sigma-Aldrich to improve the electrical conductivity of SMP nanocomposites. The 3D printer was BIOPRINTER Tissue Scribe (3mL Nozzle) purchased from 3D Cultures company.

4.3 Fabrication of 3D printed CNT/SMP nanocomposites

The procedures of 3D printed CNT/SMP nanocomposites were indicated in Figure 4-1. Certain amount of CNTs and HPED were added into a beaker which was mixed by glass rod for 10 min, then the CNTs were dispersed by probe sonication at 28% amplitude in pulse mode with

5 seconds on and 2 seconds off for 1 minute. After sonication, TEA and HDI were added to the CNT/HPED solution to prepare for the 3D printing ink.

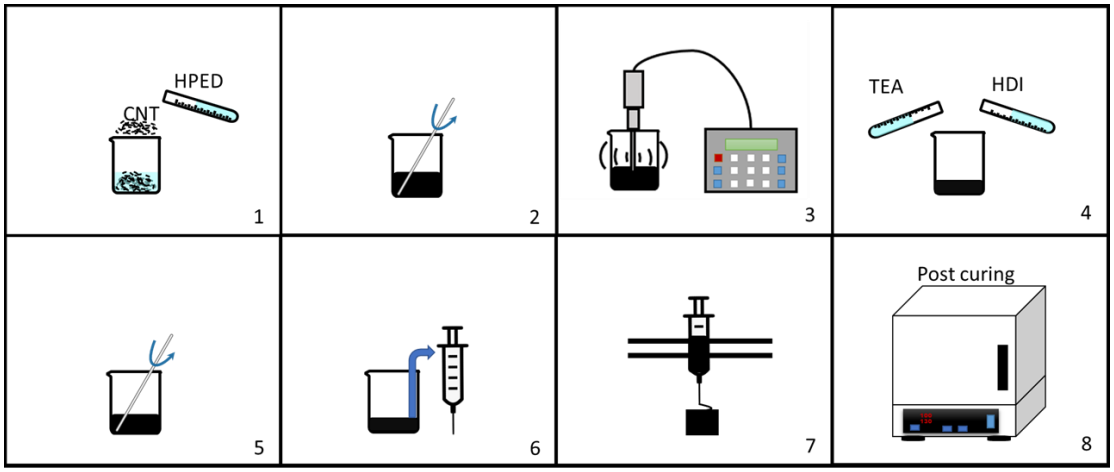

Figure 4-1 Schematic procesures of 3D printed CNT/SMP nanocomposites.

The ink was mixed by glass rod for 10 min which was transferred to a syringe. The, the syringe was mounted on the 3D printer to execute the printing process. After printing, 3D printed CNT/SMP nanocomposites were put in oven for post-curing. The curing for the nanocomposites was from room temperature to 130 °C with a ramp of 10 °C/h and held at 130 °C for 1h.

CNT/SMP nanocomposite scaffolds with a CNT fraction of 2.0 wt.%, 2.5 wt.%, 3.0 wt.%, 3.5 wt.% and 4.0 wt.% and CNT/SMP nanocomposite beams with a CNT fraction of 3.0 wt.%, were printed. The final printed nanocomposite scaffold was shown in Figure 4-2. The successful printing of scaffolds reduced the fabrication time greatly from 120h to 30 min compared to the method used in chapter 2 and 3 as the dissolving of sugar particles was time-consuming.

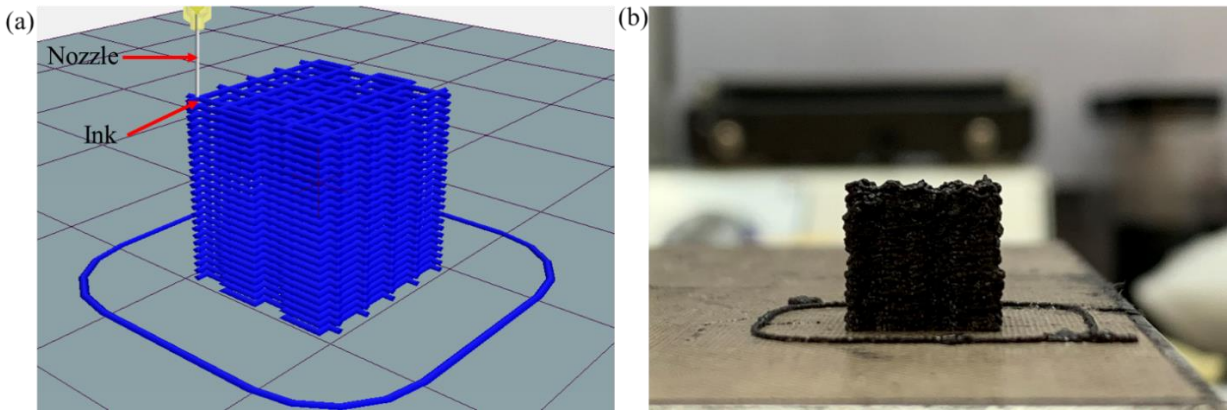

Figure 4-2 (a) Printing model of scafflod, (b) 3D printed CNT/SMP scaffold.

4.4 Characterizations

The mechanical properties of 3D printed CNT/SMP nanocomposite scaffolds were tested by the Instron 5969 universal testing system with a thermal chamber, as indicated in Figure 4-3. Cubic scaffolds with a dimension of 10mm by 10mm by 10mm were compressed to 25% strain at room temperature, T_g (39 °C) and T_g+5 (44 °C). The rate of all compression testing was 2mm/min. Before the compression testing, all the CNT/SMP nanocomposite scaffolds were preheated in the thermal chamber for 30 min to reduce the heat effect.

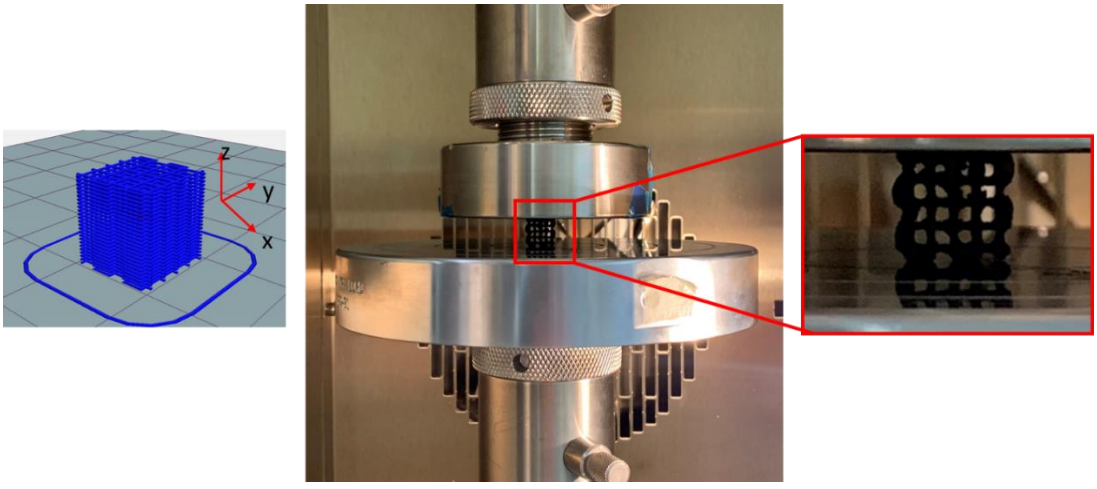

Figure 4-3 Mechanical testing setup using Instron 5969.

For measuring the electrical resistivity, 3D printed CNT/SMP nanocomposite scaffolds were dried before usage. A slight amount a silver Epoxy glue was put on the top and bottom surface of scaffold, then copper tape was attached on the surface with glue. The samples were put in room temperature for 24 hours for drying the glue. The resistivity of SMP/CNT composite scaffolds with different CNT weight concentrations was measured using electric multimeter at room temperature, T_g (39 °C), and T_g+10 (49 °C).

Thermogravimetric analysis (TGA, TA Instruments Q50) was employed to examine the thermal properties of 3D printed nanocomposites. Through the relationship between the temperature and change in mass of the specimens, the thermal stability of the sample was evaluated. Sample with a weight of near 30 mg was put inside the pan and heated under N_2 at a flow rate of 60 ml/min. The sample was heated to 900 °C with a ramp of 10 °C/min.

4.5 Optimization of 3D printing parameters

An aluminum plate covered with PTFE coated fiberglass fabric sheet was chosen as the base for printing. The fabric sheet is non-sticky to the ink and the printed nanocomposites can be easily removed from the sheet.

For printing process, the weight of ink transferred to syringe was no more than 1.5 grams. Once the transferring was ready, time was set at 0 sec. Every 5min, the quality of printed CNT/SMP nanocomposites was recorded. It was found that the maximum printing time was only 15 min as the heat generated by the reaction of ink accelerated the curing making the ink from liquid to solid which could not be squeezed out from the syringe any more.

When the weight fraction of CNTs was less than 2.5 wt.%, the viscosity of ink was too low to form a line. When the weight fraction of CNTs was over 4.0 wt.%, the highly viscous ink could

not be squeezed out from the syringe. The ink with the weight fraction of CNTs ranging from 2.5 wt.% to 4 wt.% could be printed by adjusting the infill rate and printing speed.

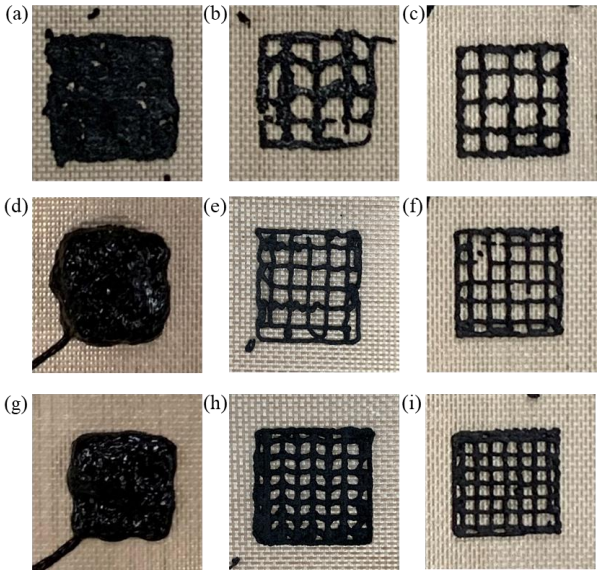

Figure 4-4 Effect of infill rate and print speed: (a) 20%&2mm/s, (b) 20%&4mm/s, (c) 20%&6mm/s, (d) 25%&2mm/s, (e) 25%&4mm/s, (f) 25%&6mm/s, (g) 30%&2mm/s, (h) 30%&4mm/s, (i) 30%&6mm/s.

Infill rate and printing speed were the two critical parameters to determine the quality of printed nanocomposites. Infill rate of 20%, 25% and 30% and printing speed of 2mm/s, 4mm/s and 6mm/s were selected, so 9 results of printed nanocomposites was shown in Figure 4-4. Based on results, it was found that higher infill rate and printing speed benefited the printing qualities.

4.6 Mechanical testing

The modulus of 3D printed CNT/SMP nanocomposite scaffolds fabricated by different weight fractions of CNTs in two different planes which were tested at different temperatures was shown in Figure 4-5.

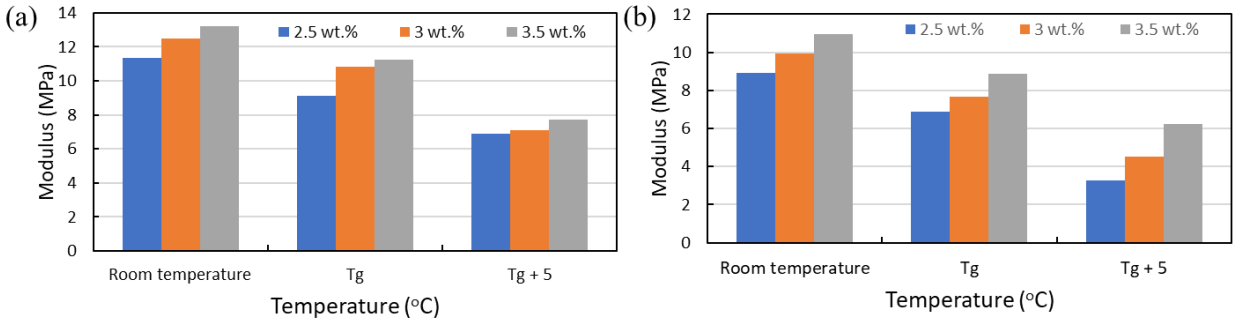

Figure 4-5 Modulus of scaffolds fabricated with different weight fractions of CNTs and tested at different temperatures :(a) in x-y plane; (b) in x-z plane.

When the temperature increased from room temperature to T_g+ 5 °C, the scaffolds became softer, so the modulus of all scaffolds decreased. The higher weight fraction of CNTs successfully enhanced the mechanical properties due to the excellent performance of CNTs including high strength and stiffness. The printing direction also influenced the mechanical performance of scaffolds as the modulus in vertical direction was higher than in x-z plane.

4.7 Thermogravimetric analysis

Thermal stability and decomposition behavior of 3D printed CNT/SMP nanocomposites were investigated by TGA as shown in Figure 4-6. There was a 1% weight loss of nanocomposites before the temperature reached to 200 °C, indicating moisture was inside. The decomposition temperature was considered as 230 °C where the weight loss sharply appeared. When the temperature increased to 550 °C, the weight loss became stable which was left only for CNTs. It was found that the high weight fraction of CNTs in nanocomposites results in higher left weight.

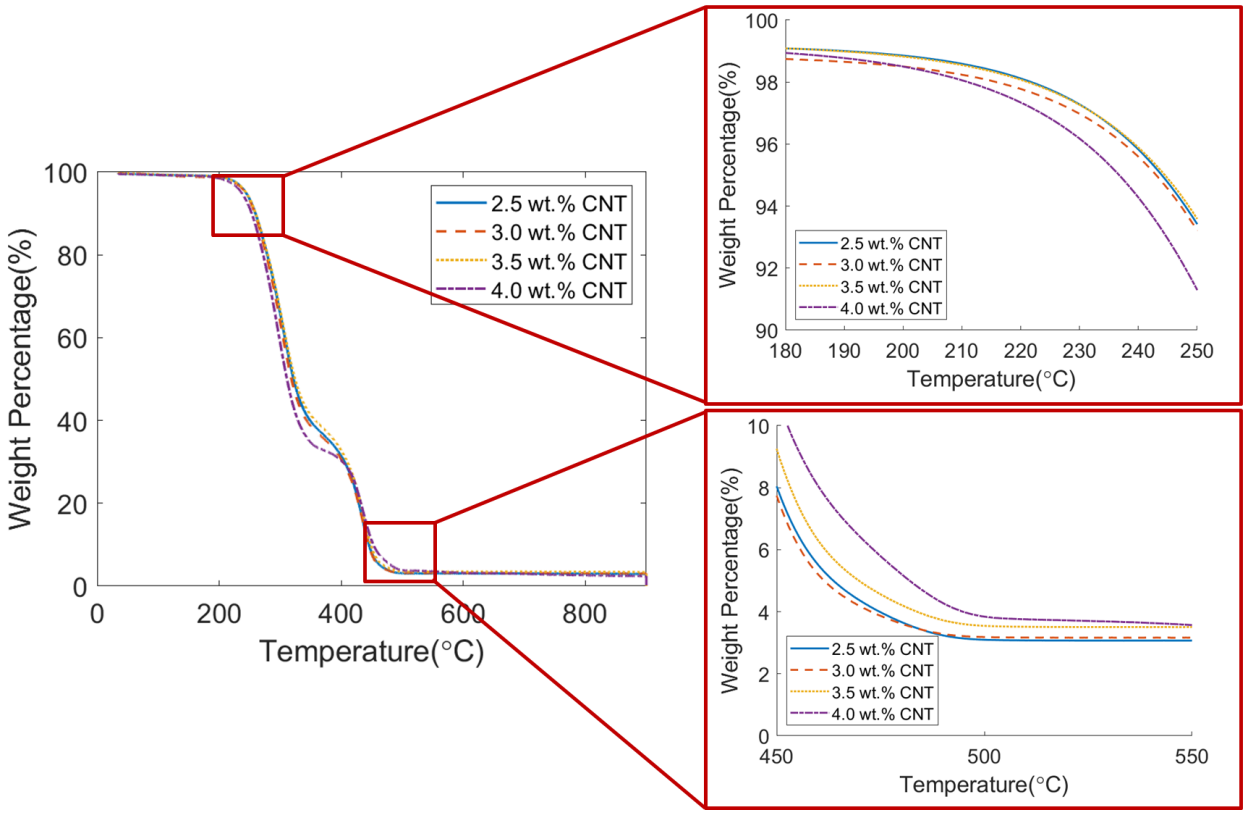

Figure 4-6 TGA results of 3D printed CNT/SMP naonocomposites with CNTs of different weight fractions.

4.8 Electrical resistivity

The effect of weight fraction of CNTs varied from 2.0 wt. % to 4.0 wt. % with an interval 0.5 wt. % on the electrical resistivity of 3D printed CNT/SMP nanocomposite scaffolds was demonstrated in Figure 4-7. When the weight ratio of CNTs in scaffold was low, the electrical conductivity was poor due to the long distance between the CNTs. The longer the distance between the fillers, the poorer conductivity would be. When the weight fraction of CNTs was above a critical value of 2.5 wt. %, the electrical conductivity became larger instantly.

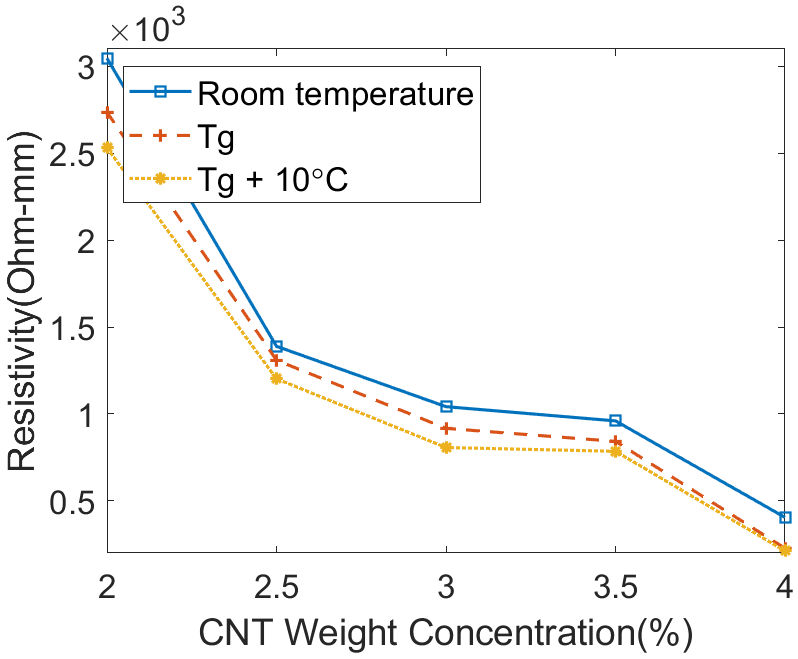

Figure 4-7 Electrical resistivity of 3D printed CNT/SMP nanocomposite scafflods with CNTs of different weight concentration.

4.9 Shape memory behavior

Electrical resistance heating was used to verify the shape recovery behavior of 3D printed CNT/SMP nanocomposite beam as shown in Figure 4-8. The beam of temporarily memorized shape that was bent about 180 degree to U like shape was fixed by two clamps which were connected to DC power. After the DC power was turned on which offered 6V voltage, the beam began to expand and recover to straight shape. The recovery time was not linear that it took about 20s to recover 90 degree but finally took about 280s to return. Compared to the original printed shape, it was not fully straight.

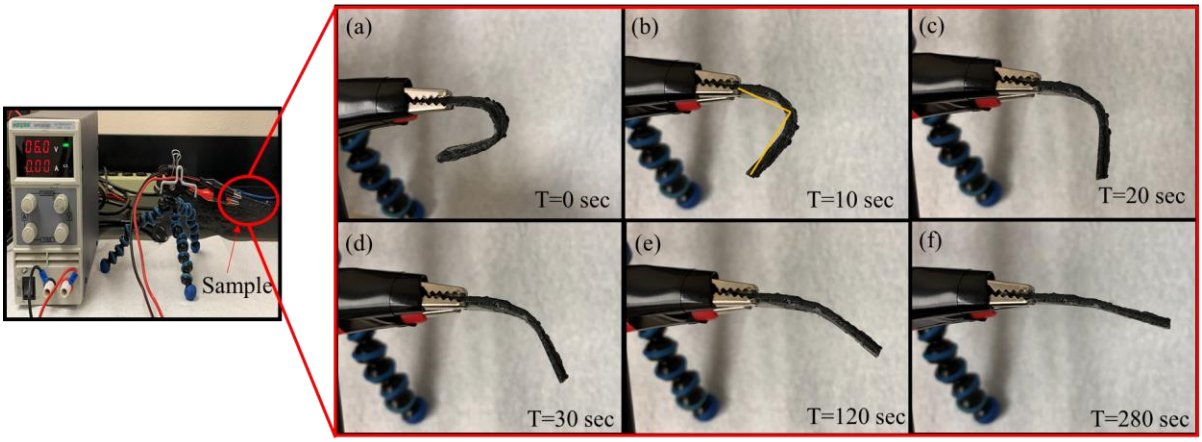

Figure 4-8 Shape recovery of 3D printed beam with 3wt. % CNT triggered by DC power.

The shape recovery effect was also investigated by direct heating using a hotplate which was demonstrated in Figure 4-9. The hotplate was pre-heated to 40 °C for 30 minutes to make the surface evenly heated. The bent beam was placed on the hot plate and the process of shape recovery was recorded. It took about 60s to recover 90 degree but finally took about 320s to return. The final shape of shape recovered beam triggered by the direct heating was similar to the result of beam by electrical resistance heating, and both of them were not fully recovered.

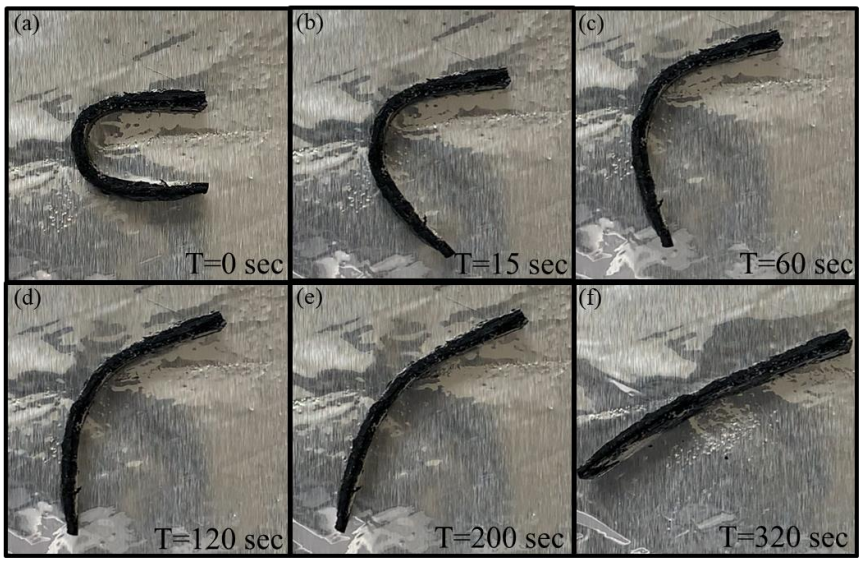

Figure 4-9 Shape recovery of 3D printed beam with 3wt. % CNT triggered by hotplate.

Chapter 5 Conclusions and Future Work

5.1 Summary

In this thesis, multiple techniques including sacrificial template and 3D printing have been used to synthesize porous SMP nanocomposites. Various properties of fabricated SMP structures were characterized including density, porosity, compression modulus, resistivity, electrical resistance heating and thermal stability. Demonstration of shape recovery behavior of SMP nanocomposites showed that this material has a potential application for treating ICAs.

Pristine SMP foams were fabricated by HPED, TEA and HDI using a sacrificial sugar template method. The shape recovery behavior of fabricated SMP foams were successfully obtained. SEM results showed that the pore size of foam was about 480um leading to a high porosity of 85.7% which had high compressive capability. For the cyclic compression test, there was a hysteresis for the material meaning the maximum stress in each cycle degreased. The current of 0.05A, 0.1A, 0.15A, and 0.2A were applied to carbon fiber which generated the heat to trigger shape recovery behavior of the foam, and 0.15A was the optimal current considering the safety of the human body.

CNTs were added using previous technique to fabricate CNT/SMP nanocomposite foams. The densities of CNT/SMP nanocomposite foams could be determined by increasing the CNT concentration or using small sugar particles. More CNTs and small sugar particles also leaded to the high modulus of foams. As CNTs were excellent conductivity materials, owing to the more involvement of CNTs, the conductivity of CNT/SMP nanocomposite foams increased greatly. The conductive foams could be heated by electrical resistance heating method to trigger the shape

recovery behavior. The prototype of embolization using CNT/SMP nanocomposite foam was successfully demonstrated in a transparent device which simulated the shape of ICAs.

3D printing technique was employed to manufacturing the customized shape of CNT/SMP nanocomposites. Printing ink was prepared by the combination of CNTs and SMP solution which had a working period for 15min. The higher infill rate and printing speed benefited the printing quality. The weight fractions of CNTs ranging from 2.5 wt.% to 4.0 wt.% combining the printing parameters of infill rate and printing speed were the value for the successful printing. Higher or lower weight fraction would lead to the failure. The involvement of 3D printing significantly reduced the synthesis time from 120h to 30 min compared to the method using sacrificial sugar template.

When more CNTs were involved in the ink, the higher modulus of 3D printed scaffolds in x-y and x-z planes could have. The TGA result indicated that the decomposition temperature of 3D printed scaffold was about 230 °C. The existing of CNTs of different weight fractions would not influence the thermal stability. Owing to the introduction of CNTs, more CNTs made the printed scaffolds have lower resistivity. The shape recovery behavior of 3D printed CNT/SMP nanocomposites was obtained based on the experiments using electrical resistance heating and direct heating. All these results prove that 3D printed porous CNT/SMP nanocomposites is very promising to be applied for the potential treatment of ICAs due to the shorter manufacturing time and convenient customization.

5.2 Future work

5.2.1 Biocompatibility

The biocompatibility of SMP synthesized by HPED, TEA and HDI has been investigated by Boyle et al. [48], while the porous SMP and CNT/SMP nanocomposites using sacrificial template and 3D printing in this study have not been done yet. Safety is always the first rule for bio-medical application, so we must make sure that this material is biocompatible and no poisonous to human body. As a result, the biocompatibility tests should be taken into consideration through the whole procedure of SMP nanocomposites synthesis and printing.

5.2.2 Investigation of using 3D printing for fabricating porous CNT/SMP nanocomposites

3D printing is a significant technique which can reduce fabrication time and realize the customization, but for our work, they are preliminary results which still have more space to improve. Photopolymer can be introduced to improve the printing resolution and accuracy. Salt or sugar particles can be also involved for the preparation of ink which lead to the porous structure of 3D printed materials.

5.2.3 Potential application in autonomous load sensing and structural health monitoring

The integration of highly conductive nanoparticles, such as graphene, CNTs, carbon black, gold nanowires , and silver nanowires, can significantly increase materials' electrical conductivity, leading to potential load sensing applications, often referred as autonomous sensing or self-sensing [92-95]. The CNT/SMP nanocomposites developed in this project can potentially be used for self-sensing, leading to external load and deformation measurement capabilities. In addition, the recorded sensing information can be used to estimate the materials' and structural integrity and embedded damage. Certain efforts have been referred as structural health monitoring and

prognostics in literature [96-103]. An example of CNT/SMP nanocomposites for structural health monitoring application is the real-time monitoring of cracks and delamination in sandwich composites by monitoring the variation of piezoresistive properties in nanocomposites. The correlation of measured resistance and potential damage provides a unique method to enhance structural safety in sandwich composites.

References

[1] Razzaq, M. Y., Anhalt, M., Frormann, L. & Weidenfeller, B. Thermal, electrical and magnetic studies of magnetite filled polyurethane shape memory polymers. *Materials Science and Engineering: A* 444, 227, (2007).

[2] Lendlein, A. & Kelch, S. Shape‐memory polymers. *Angewandte Chemie International Edition* 41, 2034, (2002).

[3] Lendlein, A., Jiang, H., Jünger, O. & Langer, R. Light-induced shape-memory polymers. *Nature* 434, 879, (2005).

[4] Gall, K., Yakacki, C. M., Liu, Y., Shandas, R., Willett, N. & Anseth, K. S. Thermomechanics of the shape memory effect in polymers for biomedical applications. *Journal of Biomedical Materials Research Part A: An Official Journal of The Society for Biomaterials, The Japanese Society for Biomaterials, and The Australian Society for Biomaterials and the Korean Society for Biomaterials* 73, 339, (2005).

[5] Liu, Y., Du, H., Liu, L. & Leng, J. Shape memory polymers and their composites in aerospace applications: a review. *Smart Materials and Structures* 23, 023001, (2014).

[6] Bao, M., Lou, X., Zhou, Q., Dong, W., Yuan, H. & Zhang, Y. Electrospun biomimetic fibrous scaffold from shape memory polymer of PDLLA-co-TMC for bone tissue engineering. *ACS applied materials & interfaces* 6, 2611, (2014).

[7] Xie, T. Tunable polymer multi-shape memory effect. *Nature* 464, 267, (2010).

[8] Leng, J., Lan, X., Liu, Y., Du, S., Huang, W., Liu, N., Phee, S. & Yuan, Q. Electrical conductivity of thermoresponsive shape-memory polymer with embedded micron sized Ni powder chains. *Applied Physics Letters* 92, 014104, (2008).

[9] Chan Vili, Y. Y. Investigating smart textiles based on shape memory materials. *Textile Research Journal* 77, 290, (2007).

[10] Ward Small, I., Singhal, P., Wilson, T. S. & Maitland, D. J. Biomedical applications of thermally activated shape memory polymers. *Journal of materials chemistry* 20, 3356, (2010).

[11] Santo, L., Quadrini, F., Accettura, A. & Villadei, W. Shape memory composites for self-deployable structures in aerospace applications. *Procedia Engineering* 88, 42, (2014).

[12] Janik, H. & Marzec, M. A review: Fabrication of porous polyurethane scaffolds. *Materials Science and Engineering: C* 48, 586, (2015).

[13] De Nardo, L., Bertoldi, S., Cigada, A., Tanzi, M. C., Haugen, H. J. & Farè, S. Preparation and characterization of shape memory polymer scaffolds via solvent casting/particulate leaching. *Journal of applied biomaterials & functional materials* 10, 119, (2012).

[14] Hendrikson, W. J., Rouwkema, J., Clementi, F., Van Blitterswijk, C. A., Farè, S. & Moroni, L. Towards 4D printed scaffolds for tissue engineering: exploiting 3D shape memory polymers to deliver time-controlled stimulus on cultured cells. *Biofabrication* 9, 031001, (2017).

[15] Mondal, S. & Hu, J. Temperature stimulating shape memory polyurethane for smart clothing. (2006).

[16] Murphy, W. L., Dennis, R. G., Kileny, J. L. & Mooney, D. J. Salt fusion: an approach to improve pore interconnectivity within tissue engineering scaffolds. *Tissue engineering* 8, 43, (2002).

[17] Singhal, P., Boyle, A., Brooks, M. L., Infanger, S., Letts, S., Small, W., Maitland, D. J. & Wilson, T. S. Controlling the actuation rate of low‐density shape‐memory polymer foams in water. *Macromolecular chemistry and physics* 214, 1204, (2013).
[18] Hasan, S. M., Nash, L. D. & Maitland, D. J. Porous shape memory polymers: Design and applications. *Journal of Polymer Science Part B: Polymer Physics* 54, 1300, (2016).
[19] Singhal, P., Small, W., Cosgriff-Hernandez, E., Maitland, D. J. & Wilson, T. S. Low density biodegradable shape memory polyurethane foams for embolic biomedical applications. *Acta biomaterialia* 10, 67, (2014).
[20] Singhal, P., Rodriguez, J. N., Small, W., Eagleston, S., Van de Water, J., Maitland, D. J. & Wilson, T. S. Ultra low density and highly crosslinked biocompatible shape memory polyurethane foams. *Journal of Polymer Science Part B: Polymer Physics* 50, 724, (2012).
[21] Wang, J., Luo, J., Kunkel, R., Saha, M., Bohnstedt, B. N., Lee, C.-H. & Liu, Y. Development of shape memory polymer nanocomposite foam for treatment of intracranial aneurysms. *Materials Letters* 250, 38, (2019).
[22] Wang, J., Kunkel, R., Luo, J., Li, Y., Liu, H., Bohnstedt, B. N., Liu, Y. & Lee, C.-H. Shape memory polyurethane with porous architectures for potential applications in intracranial aneurysm treatment. *Polymers* 11, 631, (2019).
[23] Zhang, D., George, O. J., Petersen, K. M., Jimenez-Vergara, A. C., Hahn, M. S. & Grunlan, M. A. A bioactive "self-fitting" shape memory polymer scaffold with potential to treat cranio-maxillo facial bone defects. *Acta biomaterialia* 10, 4597, (2014).
[24] De Nardo, L., Bertoldi, S., Tanzi, M. C., Haugen, H. & Fare, S. Shape memory polymer cellular solid design for medical applications. *Smart Materials and Structures* 20, 035004, (2011).
[25] Charara, M., Luo, W., Saha, M. C. & Liu, Y. Investigation of lightweight and flexible carbon nanofiber/poly dimethylsiloxane nanocomposite sponge for piezoresistive sensor application. *Advanced Engineering Materials*, 1801068, (2019).
[26] Luo, W., Charara, M., Saha, M. C. & Liu, Y. Fabrication and characterization of porous CNF/PDMS nanocomposites for sensing applications. *Applied Nanoscience* 9, 1309, (2019).
[27] Chai, Q., Huang, Y., Kirley, T. & Ayres, N. Shape memory polymer foams prepared from a heparin-inspired polyurethane/urea. *Polymer Chemistry* 8, 5039, (2017).
[28] Kashyap, D., Kumar, P. K. & Kanagaraj, S. 4D printed porous radiopaque shape memory polyurethane for endovascular embolization. *Additive Manufacturing* 24, 687, (2018).
[29] Garcia Rosales, C. A., Kim, H., Garcia Duarte, M. F., Chavez, L., Castañeda, M., Tseng, T.-L. B. & Lin, Y. Characterization of shape memory polymer parts fabricated using material extrusion 3D printing technique. *Rapid Prototyping Journal* 25, 322, (2019).
[30] Senatov, F. S., Niaza, K. V., Zadorozhnyy, M. Y., Maksimkin, A., Kaloshkin, S. & Estrin, Y. Mechanical properties and shape memory effect of 3D-printed PLA-based porous scaffolds. *Journal of the mechanical behavior of biomedical materials* 57, 139, (2016).
[31] Mu, X., Bertron, T., Dunn, C., Qiao, H., Wu, J., Zhao, Z., Saldana, C. & Qi, H. Porous polymeric materials by 3D printing of photocurable resin. *Materials Horizons* 4, 442, (2017).
[32] Li, A., Challapalli, A. & Li, G. 4D Printing of Recyclable Lightweight Architectures Using High Recovery Stress Shape Memory Polymer. *Scientific reports* 9, 7621, (2019).

[33] Abshirini, M., Charara, M., Marashizadeh, P., Saha, M. C., Altan, M. C. & Liu, Y. Functional nanocomposites for 3D printing of stretchable and wearable sensors. *Applied Nanoscience*, 1, (2019).
[34] Chavez, L. A., Wilburn, B. R., Ibave, P., Delfin, L. C., Vargas, S., Diaz, H., Fulgentes, C., Renteria, A., Regis, J. & Liu, Y. Fabrication and characterization of 3D printing induced orthotropic functional ceramics. *Smart Materials and Structures* 28, 125007, (2019).
[35] Renteria, A., Diaz, J. A., He, B., Renteria-Marquez, I. A., Chavez, L. A., Regis, J. E., Liu, Y., Espalin, D., Tseng, T.-L. B. & Lin, Y. Particle size influence on material properties of BaTiO3 ceramics fabricated using freeze-form extrusion 3D printing. *Materials Research Express* 6, 115211, (2019).
[36] Wang, J., Golly, N. C., Herren, B., Liu, Y., Macdonald, J. I. & Siddique, Z. in *2019 ASEE Annual Conference & Exposition.*
[37] Chavez, L. A., Regis, J. E., Delfin, L. C., Garcia Rosales, C. A., Kim, H., Love, N., Liu, Y. & Lin, Y. Electrical and mechanical tuning of 3D printed photopolymer–MWCNT nanocomposites through in situ dispersion. *Journal of Applied Polymer Science* 136, 47600, (2019).
[38] Renteria, A., Fontes, H., Diaz, J. A., Regis, J. E., Chavez, L. A., Tseng, T.-L. B., Liu, Y. & Lin, Y. Optimization of 3D printing parameters for BaTiO3 piezoelectric ceramics through design of experiments. *Materials Research Express* 6, 085706, (2019).
[39] Mondal, A., Sukati, M., Charara, M., Saha, M., Liu, Y., Patterson, S. & Robison, T. in *Proceedings of the American Society for Composites—Thirty-fourth Technical Conference.*
[40] Abshirini, M., Charara, M., Liu, Y., Saha, M. C. & Altan, M. C. in *ASME 2018 International Mechanical Engineering Congress and Exposition.* (American Society of Mechanical Engineers Digital Collection).
[41] Abshirini, M., Charara, M., Liu, Y., Saha, M. & Altan, M. C. 3D printing of highly stretchable strain sensors based on carbon nanotube nanocomposites. *Advanced Engineering Materials* 20, 1800425, (2018).
[42] Wang, J., Lee, D. & Liu, Y. in *ASME 2017 International Mechanical Engineering Congress and Exposition.* (American Society of Mechanical Engineers Digital Collection).
[43] Santo, L. in *Materials Science Forum.* 165 (Trans Tech Publ).
[44] Santo, L. Shape memory polymer foams. *Progress in Aerospace Sciences* 81, 60, (2016).
[45] Sokolowski, W., Tan, S. & Pryor, M. in *45th AIAA/ASME/ASCE/AHS/ASC Structures, Structural Dynamics & Materials Conference.* 1660.
[46] Fabrizio, Q., Loredana, S. & Anna, S. E. Shape memory epoxy foams for space applications. *Materials letters* 69, 20, (2012).
[47] De Nardo, L., Alberti, R., Cigada, A., Yahia, L. H., Tanzi, M. C. & Farè, S. Shape memory polymer foams for cerebral aneurysm reparation: effects of plasma sterilization on physical properties and cytocompatibility. *Acta biomaterialia* 5, 1508, (2009).
[48] Boyle, A. J., Landsman, T. L., Wierzbicki, M. A., Nash, L. D., Hwang, W., Miller, M. W., Tuzun, E., Hasan, S. M. & Maitland, D. J. In vitro and in vivo evaluation of a shape memory polymer foam‐over‐wire embolization device delivered in saccular aneurysm models. *Journal of Biomedical Materials Research Part B: Applied Biomaterials* 104, 1407, (2016).

[49] Kai, D., Prabhakaran, M. P., Chan, B. Q. Y., Liow, S. S., Ramakrishna, S., Xu, F. & Loh, X. J. Elastic poly (ε-caprolactone)-polydimethylsiloxane copolymer fibers with shape memory effect for bone tissue engineering. *Biomedical Materials* 11, 015007, (2016).
[50] Xie, M., Wang, L., Ge, J., Guo, B. & Ma, P. X. Strong electroactive biodegradable shape memory polymer networks based on star-shaped polylactide and aniline trimer for bone tissue engineering. *ACS applied materials & interfaces* 7, 6772, (2015).
[51] Huang, W. M., Song, C., Fu, Y. Q., Wang, C. C., Zhao, Y., Purnawali, H., Lu, H., Tang, C., Ding, Z. & Zhang, J. Shaping tissue with shape memory materials. *Advanced Drug Delivery Reviews* 65, 515, (2013).
[52] Seibert, B., Tummala, R., Chow, R., Faridar, A., Mousavi, S. A. & Divani, A. A. Intracranial aneurysms: review of current treatment options and outcomes. *Frontiers in neurology* 2, 45, (2011).
[53] Rinkel, G. J., Djibuti, M., Algra, A. & Van Gijn, J. Prevalence and risk of rupture of intracranial aneurysms: a systematic review. *Stroke* 29, 251, (1998).
[54] Ducruet, A. F., Hickman, Z. L., Zacharia, B. E., Narula, R., Grobelny, B. T., Gorski, J. & Connolly, E. S. Intracranial infectious aneurysms: a comprehensive review. *Neurosurgical review* 33, 37, (2010).
[55] Naggara, O. N., White, P. M., Guilbert, F., Roy, D., Weill, A. & Raymond, J. Endovascular treatment of intracranial unruptured aneurysms: systematic review and meta-analysis of the literature on safety and efficacy. *Radiology* 256, 887, (2010).
[56] Huang, J., McGirt, M. J., Gailloud, P. & Tamargo, R. J. Intracranial aneurysms in the pediatric population: case series and literature review. *Surgical neurology* 63, 424, (2005).
[57] Forget Jr, T. R., Benitez, R., Veznedaroglu, E., Sharan, A., Mitchell, W., Silva, M. & Rosenwasser, R. H. A review of size and location of ruptured intracranial aneurysms. *Neurosurgery* 49, 1322, (2001).
[58] Hampikian, J. M., Heaton, B. C., Tong, F. C., Zhang, Z. & Wong, C. Mechanical and radiographic properties of a shape memory polymer composite for intracranial aneurysm coils. *Materials Science and Engineering: C* 26, 1373, (2006).
[59] Maitland, D. J., Metzger, M. F., Schumann, D., Lee, A. & Wilson, T. S. Photothermal properties of shape memory polymer micro‐actuators for treating stroke. *Lasers in Surgery and Medicine: The Official Journal of the American Society for Laser Medicine and Surgery* 30, 1, (2002).
[60] Maitland, D. J., Small, W., Ortega, J. M., Buckley, P. R., Rodriguez, J., Hartman, J. & Wilson, T. S. Prototype laser-activated shape memory polymer foam device for embolic treatment of aneurysms. *Journal of biomedical optics* 12, 030504, (2007).
[61] Rodriguez, J. N., Yu, Y.-J., Miller, M. W., Wilson, T. S., Hartman, J., Clubb, F. J., Gentry, B. & Maitland, D. J. Opacification of shape memory polymer foam designed for treatment of intracranial aneurysms. *Annals of biomedical engineering* 40, 883, (2012).
[62] Kunkel, R., Laurence, D., Wang, J., Robinson, D., Scherrer, J., Wu, Y., Bohnstedt, B., Chien, A., Liu, Y. & Lee, C.-H. Synthesis and characterization of bio-compatible shape memory polymers with potential applications to endovascular embolization of intracranial aneurysms. *Journal of the mechanical behavior of biomedical materials* 88, 422, (2018).

[63] Wang, J., Chowdhury, S., Liu, Y., Bohnstedt, B. & Lee, C.-H. in *ASME 2017 International Mechanical Engineering Congress and Exposition.* (American Society of Mechanical Engineers Digital Collection).
[64] Wang, J., Luo, J., Kunkel, R., Liu, Y., Bohnstedt, B. & Lee, C.-H. in *ASME 2018 International Mechanical Engineering Congress and Exposition.* (American Society of Mechanical Engineers Digital Collection).
[65] Dandy, W. E. Intracranial aneurysm of the internal carotid artery - Cured by operation. *Annals of Surgery* 107, 654, (1938).
[66] Murayama, Y., Nien, Y. L., Duckwiler, G., Gobin, Y. P., Jahan, R., Frazee, J., Martin, N. & Viñuela, F. Guglielmi detachable coil embolization of cerebral aneurysms: 11 years' experience. *Journal of neurosurgery* 98, 959, (2003).
[67] Zubillaga, A. F., Guglielmi, G., Vinuela, F. & Duckwiler, G. R. Endovascular occlusion of intracranial aneurysms with electrically detachable coils: correlation of aneurysm neck size and treatment results. *American Journal of Neuroradiology* 15, 815, (1994).
[68] Hayakawa, M., Murayama, Y., Duckwiler, G. R., Gobin, Y. P., Guglielmi, G. & Viñuela, F. Natural history of the neck remnant of a cerebral aneurysm treated with the Guglielmi detachable coil system. *Journal of neurosurgery* 93, 561, (2000).
[69] Sluzewski, M., Bosch, J. A., van Rooij, W. J., Nijssen, P. C. & Wijnalda, D. Rupture of intracranial aneurysms during treatment with Guglielmi detachable coils: incidence, outcome, and risk factors. *Journal of neurosurgery* 94, 238, (2001).
[70] Gobin, Y. P., Viñuela, F., Gurian, J. H., Guglielmi, G., Duckwiler, G. R., Massoud, T. F. & Martin, N. A. Treatment of large and giant fusiform intracranial aneurysms with Guglielmi detachable coils. *Journal of neurosurgery* 84, 55, (1996).
[71] Cloft, H. J. & Kallmes, D. F. Cerebral aneurysm perforations complicating therapy with Guglielmi detachable coils: a meta-analysis. *American Journal of Neuroradiology* 23, 1706, (2002).
[72] Gallas, S., Pasco, A., Cottier, J.-P., Gabrillargues, J., Drouineau, J., Cognard, C. & Herbreteau, D. A multicenter study of 705 ruptured intracranial aneurysms treated with Guglielmi detachable coils. *American Journal of Neuroradiology* 26, 1723, (2005).
[73] Small, W., Buckley, P. R., Wilson, T. S., Benett, W. J., Hartman, J., Saloner, D. & Maitland, D. J. Shape memory polymer stent with expandable foam: a new concept for endovascular embolization of fusiform aneurysms. *IEEE Transactions on Biomedical Engineering* 54, 1157, (2007).
[74] Hwang, W., Volk, B. L., Akberali, F., Singhal, P., Criscione, J. C. & Maitland, D. J. Estimation of aneurysm wall stresses created by treatment with a shape memory polymer foam device. *Biomechanics and modeling in mechanobiology* 11, 715, (2012).
[75] Meng, H. & Li, G. A review of stimuli-responsive shape memory polymer composites. *Polymer* 54, 2199, (2013).
[76] Liu, T., Zhou, T., Yao, Y., Zhang, F., Liu, L., Liu, Y. & Leng, J. Stimulus methods of multi-functional shape memory polymer nanocomposites: A review. *Composites Part A: Applied Science and Manufacturing* 100, 20, (2017).
[77] Liu, Y., Lv, H., Lan, X., Leng, J. & Du, S. Review of electro-active shape-memory polymer composite. *Composites Science and Technology* 69, 2064, (2009).
[78] Meng, Q. & Hu, J. A review of shape memory polymer composites and blends. *Composites Part A: Applied Science and Manufacturing* 40, 1661, (2009).

[79] Rousseau, I. A. Challenges of shape memory polymers: A review of the progress toward overcoming SMP's limitations. *Polymer Engineering & Science* 48, 2075, (2008).
[80] Luo, W., Liu, Y. & Saha, M. in *ASME 2017 international mechanical engineering congress and exposition.* (American Society of Mechanical Engineers Digital Collection).
[81] Chowdhury, S. A., Saha, M. C., Patterson, S., Robison, T. & Liu, Y. Highly conductive polydimethylsiloxane/carbon nanofiber composites for flexible sensor applications. *Advanced Materials Technologies* 4, 1800398, (2019).
[82] Ni, Q.-Q., Zhang, C.-s., Fu, Y., Dai, G. & Kimura, T. Shape memory effect and mechanical properties of carbon nanotube/shape memory polymer nanocomposites. *Composite Structures* 81, 176, (2007).
[83] Kiyatkin, E. A. Brain temperature homeostasis: physiological fluctuations and pathological shifts. *Frontiers in bioscience: a journal and virtual library* 15, 73, (2010).
[84] Wang, H., Wang, B., Normoyle, K. P., Jackson, K., Spitler, K., Sharrock, M. F., Miller, C. M., Best, C., Llano, D. & Du, R. Brain temperature and its fundamental properties: a review for clinical neuroscientists. *Frontiers in neuroscience* 8, 307, (2014).
[85] Small, W., Singhal, P., Wilson, T. S. & Maitland, D. J. Biomedical applications of thermally activated shape memory polymers. *Journal of Materials Chemistry* 20, 3356, (2010).
[86] Hu, J., Zhu, Y., Huang, H. & Lu, J. Recent advances in shape–memory polymers: Structure, mechanism, functionality, modeling and applications. *Progress in Polymer Science* 37, 1720, (2012).
[87] Li, G. & Nettles, D. Thermomechanical characterization of a shape memory polymer based self-repairing syntactic foam. *Polymer* 51, 755, (2010).
[88] Ohki, T., Ni, Q.-Q., Ohsako, N. & Iwamoto, M. Mechanical and shape memory behavior of composites with shape memory polymer. *Composites Part A: applied science and manufacturing* 35, 1065, (2004).
[89] Easley, A. D., Monroe, M. B. B., Hasan, S. M., Weems, A. C., Frederick, J. & Maitland, D. J. Shape memory polyurethane‐urea foams with improved toughness. *J Appl Polym Sci* 136, 47268, (2019).
[90] Zhang, C.-S., Ni, Q.-Q., Fu, S.-Y. & Kurashiki, K. Electromagnetic interference shielding effect of nanocomposites with carbon nanotube and shape memory polymer. *Composites Science and Technology* 67, 2973, (2007).
[91] Leng, J., Lan, X., Liu, Y. & Du, S. Electroactive thermoset shape memory polymer nanocomposite filled with nanocarbon powders. *Smart Materials and Structures* 18, 074003, (2009).
[92] Zou, J., Liu, Y., Chattopadhyay, A. & Dai, L. in *Behavior and Mechanics of Multifunctional Materials and Composites 2015.* 943204 (International Society for Optics and Photonics).
[93] Zou, J., Liu, Y., Shan, B., Chattopadhyay, A. & Dai, L. L. Early damage detection in epoxy matrix using cyclobutane-based polymers. *Smart Materials and Structures* 23, 095038, (2014).
[94] Liu, Y., Rajadas, A. & Chattopadhyay, A. in *ASME 2013 Conference on Smart Materials, Adaptive Structures and Intelligent Systems.* (American Society of Mechanical Engineers Digital Collection).

[95] Liu, Y., Rajadas, A. & Chattopadhyay, A. A biomimetic structural health monitoring approach using carbon nanotubes. *Jom* 64, 802, (2012).
[96] Liu, Y., Mohanty, S. & Chattopadhyay, A. Condition based structural health monitoring and prognosis of composite structures under uniaxial and biaxial loading. *Journal of Nondestructive Evaluation* 29, 181, (2010).
[97] Liu, Y., Kim, S. B. & Chattopadhyay, A. in *51st AIAA/ASME/ASCE/AHS/ASC Structures, Structural Dynamics, and Materials Conference 18th AIAA/ASME/AHS Adaptive Structures Conference 12th.* 3027.
[98] Liu, Y., Fard, M., Kim, S., Chattopadhyay, A. & Doyle, D. in *52nd AIAA/ASME/ASCE/AHS/ASC Structures, Structural Dynamics and Materials Conference 19th AIAA/ASME/AHS Adaptive Structures Conference 13t.* 1859.
[99] Liu, Y., Fard, M. Y., Kim, S. B., Chattopadhyay, A. & Doyle, D. in *Sensors and Smart Structures Technologies for Civil, Mechanical, and Aerospace Systems 2011.* 79813N (International Society for Optics and Photonics).
[100] Liu, Y., Kim, S. B., Chattopadhyay, A. & Doyle, D. T. Application of system-identification techniquest to health monitoring of on-orbit satellite boom structures. *Journal of Spacecraft and Rockets* 48, 589, (2011).
[101] Liu, Y., Fard, M. Y., Chattopadhyay, A. & Doyle, D. Damage assessment of CFRP composites using a time–frequency approach. *Journal of Intelligent Material Systems and Structures* 23, 397, (2012).
[102] Liu, Y. & Nayak, S. Structural health monitoring: State of the art and perspectives. *Jom* 64, 789, (2012).
[103] Liu, Y. & Chattopadhyay, A. Low-velocity impact damage monitoring of a sandwich composite wing. *Journal of Intelligent Material Systems and Structures* 24, 2074, (2013).